Global impacts of gas-phase chemistry-aerosol interactions on direct radiative forcing by anthropogenic aerosols and ozone

Hong Liao and John H. Seinfeld

Division of Engineering and Applied Science and Department of Chemical Engineering, California Institute of Technology, Pasadena, California, USA

Received 22 February 2005; revised 10 June 2005; accepted 24 July 2005; published 27 September 2005.

[1] We present here a first global modeling study on the influence of gas-phase chemistry/aerosol interactions on estimates of anthropogenic forcing by tropospheric O_3 and aerosols. Concentrations of gas-phase species and sulfate, nitrate, ammonium, black carbon, primary organic carbon, secondary organic carbon, sea salt, and mineral dust aerosols in the preindustrial, present-day, and year 2100 (IPCC SRES A2) atmospheres are simulated online in the Goddard Institute for Space Studies general circulation model II' (GISS GCM II'). With fully coupled chemistry and aerosols, the preindustrial, present-day, and year 2100 global burdens of tropospheric ozone are predicted to be 190, 319, and 519 Tg, respectively. The burdens of sulfate, nitrate, black carbon, and organic carbon are predicted respectively to be 0.32. 0.18, 0.01, 0.33 Tg in preindustrial time, 1.40, 0.48, 0.23, 1.60 Tg in present-day, and 1.37, 1.97, 0.54, 3.31 Tg in year 2100. Anthropogenic O_3 is predicted to have a globally and annually averaged present-day forcing of +0.22 W m^{-2} and year 2100 forcing of +0.57 W m^{-2} at the top of the atmosphere (TOA). Net anthropogenic TOA forcing by internally mixed sulfate, nitrate, organic carbon, and black carbon aerosols is estimated to be virtually zero in the present-day and +0.34 W m^{-2} in year 2100, whereas it is predicted to be -0.39 W m^{-2} in present-day and -0.61 W m^{-2} in year 2100 if the aerosols are externally mixed. Heterogeneous reactions are shown to be important in affecting anthropogenic forcing. When reactions of N_2O_5, NO_3, NO_2, and HO_2 on aerosols are accounted for, TOA anthropogenic O_3 forcing is less by 20–45% in present-day and by 20–32% in year 2100 at mid to high latitudes in the Northern Hemisphere, as compared with values predicted in the absence of heterogeneous gas-aerosol reactions. Mineral dust uptake of HNO_3 and O_3 is shown to have practically no influence on anthropogenic O_3 forcing. Heterogeneous reactions of N_2O_5, NO_3, NO_2, and HO_2 are predicted to have noticeable impacts on anthropogenic aerosol forcing over industrialized areas, leading to 0–2 W m^{-2} more anthropogenic aerosol cooling in present-day and 2–8 W m^{-2} more cooling in year 2100 in these areas as compared with forcings calculated in the absence of heterogeneous reactions. Sea salt uptake of SO_2 reduces the magnitude of TOA aerosol cooling by 0.5–1 W m^{-2} over the oceans around 60°N in the present-day and year 2100 scenarios. Near dust sources, mineral dust uptake of SO_2 and HNO_3 leads to less anthropogenic aerosol cooling by 0.5–1 W m^{-2} in the present-day and 1–2 W m^{-2} in year 2100.

Citation: Liao, H., and J. H. Seinfeld (2005), Global impacts of gas-phase chemistry-aerosol interactions on direct radiative forcing by anthropogenic aerosols and ozone, *J. Geophys. Res.*, *110*, D18208, doi:10.1029/2005JD005907.

1. Introduction

[2] Scattering and absorption of radiation by tropospheric O_3 and aerosols are key processes in influencing global radiative forcing [*Intergovernmental Panel on Climate Change* (*IPCC*), 2001]. Major aerosol species in the atmosphere include sulfate, nitrate, black carbon (BC), organic carbon (OC), sea salt, and mineral dust. Numerous studies have estimated global radiative forcing by individual aerosol components, such as sulfate [e.g., *Boucher and Anderson*, 1995; *Feichter et al.*, 1997; *Penner et al.*, 1998; *Koch et al.*, 1999; *Kiehl et al.*, 2000], carbonaceous aerosols [e.g., *Schult et al.*, 1997; *Penner et al.*, 1998; *Cooke et al.*, 1999; *Koch*, 2001; *Chung and Seinfeld*, 2002], sea salt [*Gong et al.*, 1997; *Grini et al.*, 2002], and mineral dust [*Tegen and Lacis*, 1996; *Woodward*, 2001]. Multiple aerosol components have also been simulated simultaneously in global models [*Tegen et al.*, 2000; *Adams et al.*, 2001; *Ghan et al.*, 2001; *Jacobson*, 2001; *Wilson et al.*, 2001; *Collins et al.*, 2001; *Chin et al.*, 2002; *Metzger et al.*, 2002a, 2002b; *Takemura et al.*, 2002; *Derwent et al.*, 2003; *Liao et al.*, 2003, 2004]. No study has

0148-0227/05/2005JD005907$09.00

yet addressed how gas-phase chemistry-aerosol interactions influence the estimates of direct radiative forcing by anthropogenic O_3 and aerosols in the troposphere.

[3] Atmospheric aerosols and gas-phase chemistry interact. On one hand, gas-phase species govern many aspects of the formation and growth of aerosols. For example, the concentrations of O_3 and H_2O_2 determine the oxidation of SO_2 to form sulfate aerosol, and the partitioning of HNO_3 between the gas and aerosol phases governs the level of nitrate aerosol. One the other hand, aerosols impact gas-phase atmospheric chemistry by altering photolysis rates [*Demerjian et al.*, 1980; *Ruggaber et al.*, 1994; *Lantz et al.*, 1996; *Castro et al.*, 1997; *Landgraf and Crutzen*, 1998; *Dickerson et al.*, 1997; *Jacobson*, 1998; *Liao et al.*, 1999; *Martin et al.*, 2003; *Bian and Zender*, 2003] and by serving as sites for heterogeneous conversion of gas-phase species [*Dentener and Crutzen*, 1993; *Andreae and Crutzen*, 1997; *Jacob*, 2000]. The global effect of aerosols on gas-phase chemistry through altered photolysis rates is small; *Liao et al.* [2003] found that accounting for the effects of aerosols on photolysis rates changes global O_3 concentrations by less than 1 ppbv. *Fiore et al.* [2003] showed that the inclusion of aerosols in photolysis rate calculations changes monthly mean O_3 by less than 0.2 ppbv anywhere, and *Bian and Zender* [2003] reported that the impact of mineral dust aerosol on photolysis rates leads to a global increase in predicted O_3 concentrations of about 0.2% on a global and annual mean basis.

[4] Heterogeneous processes are predicted to be important in influencing atmospheric compositions [*Dentener and Crutzen*, 1993; *Dentener et al.*, 1996; *Zhang and Carmichael*, 1999; *Song and Carmichael*, 2001; *Bauer et al.*, 2004; *Liao et al.*, 2003, 2004]. *Dentener and Crutzen* [1993] predicted that heterogeneous reactions of NO_3 and N_2O_5 on sulfate aerosol particles can reduce the global tropospheric average O_3 burden by about 9%. *Liao et al.* [2004] showed that ignoring heterogeneous reactions may lead to predicted increases in burdens of tropospheric sulfate, nitrate, and O_3 by 28%, 50%, and 16%, respectively.

[5] In this study we explore the extent to which the chemistry-aerosol interactions influence assessments of anthropogenic direct radiative forcing. This builds on our previous work [*Liao et al.*, 2003, 2004], in which we have developed a unified tropospheric chemistry-aerosol model within the Goddard Institute for Space Studies general circulation model (GISS GCM); the model includes a detailed simulation of tropospheric O_3-NO_x-hydrocarbon chemistry, as well as aerosols and aerosol precursors. Predicted aerosol species include sulfate, nitrate, ammonium, black carbon, primary organic carbon, secondary organic carbon, sea salt, and mineral dust. Two-way coupling between aerosols and chemistry provides on-line consistent chemical fields for aerosol dynamics and aerosol mass for heterogeneous processes and calculations of gas-phase photolysis rates. Here we investigate the effect of chemistry-aerosol coupling on estimates of direct radiative forcing by tropospheric O_3 and aerosols for the years 1800 (preindustrial), 2000, and 2100 (IPCC SRES A2) [*Nakicenovic et al.*, 2000]. We choose to simulate the A2 Scenario for 2100 because it exhibits the largest changes in emissions of precursors of O_3 and aerosols; consequently, the results presented in this work can be taken to represent an upper limit estimate of the influence of chemistry-aerosol interactions on radiative forcing estimates over the next century.

2. Methodology

2.1. Model Description

[6] We use the GISS GCM II' [*Rind and Lerner*, 1996; *Rind et al.*, 1999] with online simulation of O_3-NO_x-hydrocarbon chemistry and aerosols. The model has a resolution of 4° latitude by 5° longitude, with 9 vertical layers in a σ-coordinate system extending from the surface to 10 mbar. The version of the GCM used for this study uses monthly mean ocean temperature maps. The GISS radiation scheme uses the single Gauss point doubling/adding radiative transfer model [*Lacis and Hansen*, 1974; *Hansen et al.*, 1983; *Lacis and Mishchenko*, 1995] and uses the correlated *k*-distribution method to compute absorption by gases for 6 solar and 25 thermal intervals [*Lacis and Oinas*, 1991]. Gas-phase absorbers in the longwave include H_2O, CO_2, N_2O, CH_4, and O_3, and in the shortwave H_2O, CO_2, NO_2, O_2, and O_3. Prescribed climatological distributions of O_3 and aerosols are used in the radiative calculations that drive the GCM meteorology. The radiative forcing calculation does not feed back into the GCM climate; the simulations for the years 1800, 2000, and 2100 use exactly the same meteorological fields.

[7] The model includes a detailed simulation of tropospheric O_3-NO_x-hydrocarbon chemistry and the prediction of sulfate/nitrate/ammonium/sea salt/water, black carbon, primary organic carbon, secondary organic carbon, and mineral dust aerosols. The chemistry scheme includes 225 chemical species and 346 reactions. We use 24 tracers in the model to describe O_3-NO_x-hydrocarbon chemistry, including odd oxygen ($O_x = O_3 + O + NO_2 + 2NO_3$), NO_x ($NO + NO_2 + NO_3 + HNO_2$), N_2O_5, HNO_3, HNO_4, peroxyacetyl nitrate, H_2O_2, CO, C_3H_8, C_2H_6, ($\geq C_4$) alkanes, ($\geq C_3$) alkenes, isoprene, acetone, CH_2O, CH_3CHO, CH_3OOH, ($\geq C_3$) aldehydes, ($\geq C_4$) ketones, methyl vinyl ketone, methacrolein, peroxymethacryloyl nitrate, lumped peroxyacyl nitrates, and lumped alkyl nitrates. Aerosol related mass concentrations include SO_2, SO_4^{2-}, dimethyl sulfide (DMS), NH_3, NH_4^+, NO_3^-, sea salt in 11 size bins (0.031–0.063, 0.063–0.13, 0.13–0.25, 0.25–0.5, 0.5–1, 1–2, 2–4, 4–8, 8–16, 16–32, 32–64 μm dry radius), mineral dust in 6 size bins (0.0316–0.1, 0.1–0.316, 0.316–1.0, 1.0–3.16, 3.16–10, and 10–31.6 μm dry radius), BC, primary organic carbon, as well as 5 classes of reactive hydrocarbons and 28 organic oxidation products for secondary organic carbon aerosol (SOA) formation. The chemistry scheme and 88 tracers transported in the GCM are given in *Liao et al.* [2003, 2004].

[8] Aerosol dynamics and composition are treated with a simple bulk model of internally mixed SO_4^{2-}, NH_4^+, NO_3^-, sea salt, and H_2O. This mixture is assumed to reach equilibrium with the gas-phase, which is represented by the aerosol thermodynamics module, ISORROPIA [*Nenes et al.*, 1998], to determine the partitioning of NH_3 and HNO_3 between the gas and aerosol phases and to calculate water associated with each of sulfate, nitrate, and sea salt aerosols. The formation of secondary organic aerosols is based on equilibrium partitioning and experimentally deter-

Table 1. Uptake Coefficients for Heterogeneous Reactions and the Definitions of Baseline and Sensitivity Simulations

Reactions	On Medium	Uptake Coefficients	References	Simulations			
				Baseline	NOHET	HETNODUST	HETDUST
$N_2O_5 \rightarrow 2HNO_3$	Sulfate/nitrate/ ammonium	equation (1) (see text)	*Kane et al.* [2001], *Hallquist et al.* [2003]	Yes	No	Yes	No
	Organic carbon	0.03 (RH $\geq$ 57)[a] $5.2 \times 10^{-4} \times$ RH (RH < 57)	*Thornton et al.* [2003]				
	Sea salt	0.03 (RH $\geq$ 50) 0.005 (RH < 50)	*Atkinson et al.* [2004]				
	Mineral dust	$4.25 \times 10^{-4} \times$ RH-9.75×10^{-3}	*Bauer et al.* [2004]				
$NO_3 \rightarrow HNO_3$	Wet aerosols[b]	0.001	*Jacob* [2000]	Yes	No	Yes	No
$NO_2 \rightarrow 0.5HNO_3 + 0.5HNO_2$	Wet aerosols[b]	0.0001	*Jacob* [2000]	Yes	No	Yes	No
$HO_2 \rightarrow 0.5H_2O_2$	Wet aerosols[b]	0.2	*Jacob* [2000]	Yes	No	Yes	No
$SO_2 \rightarrow SO_4^{2-}$ (dust)	Mineral dust	3×10^{-4} (RH < 50) 0.1 (RH $\geq$ 50)	*Dentener et al.* [1996]	Yes	No	No	Yes
$HNO_3 \rightarrow NO_3^-$ (dust)	Mineral dust	0.1	*Bauer et al.* [2004]	Yes	No	No	Yes
$O_3 \rightarrow$ products	Mineral dust	10^{-5}	*Bauer et al.* [2004]	Yes	No	No	Yes
$SO_2 \rightarrow SO_4^{2-}$	Sea Salt	0.05 (RH $\geq$ 50) 0.005 (RH < 50)	*Song and Carmichael* [2001]	Yes	No	Yes	No

[a]RH in percent.
[b]$SO_4^{2-}/NO_3^-/NH_4^+/NaCl/H_2O$, OC, sea salt, and mineral dust aerosols are considered to be wet when RH $\geq$ 50.

mined parameters [*Griffin et al.*, 1999a, 1999b; *Chung and Seinfeld*, 2002].

[9] The model simulates both wet and dry deposition. Dry deposition is computed with the resistance-in-series scheme of *Wesely* [1989] for all the tracers except carbonaceous aerosols, for which a deposition velocity of 0.1 cm s^{-1} is assumed [*Liousse et al.*, 1996; *Chung and Seinfeld*, 2002]. The wet deposition scheme is that reported by *Koch et al.* [1999]. Wet deposition of dissolved tracers is treated separately for large-scale and convective clouds, following the GCM cloud schemes described in *Del Genio and Yao* [1993] and *Del Genio et al.* [1996]. Dissolved gases and aerosols are scavenged within and below precipitating clouds. The solubility of gases is determined by their effective Henry's law constants. Sulfate, ammonium, nitrate, sea salt, and hydrophilic POA and BC are assumed to be fully soluble. For SOA, 80% is assumed to dissolve into clouds, consistent with findings of *Limbeck and Puxbaum* [2000]. We use a scavenging coefficient of 0.1 for dust nucleation scavenging within clouds to account for the hydrophobic nature of mineral aerosol [*Zender et al.*, 2003]. We also account for the scavenging of HNO_3 by ice clouds [*Liao et al.*, 2003].

[10] The model used in this work is basically the same as that described in *Liao et al.* [2004], except that we have updated the GISS GCM II' to a newer version with a q-flux ocean appropriate for climate simulations. This update has minor influences on predicted gas-phase species and aerosols, since we still use monthly mean ocean temperature maps in this work. We have updated the size distribution of emitted dust particles from the distribution in *Woodward* [2001] to that in *Zender et al.* [2003] to achieve better agreement of predicted optical depths with measurements. The updates in heterogeneous reactions and emission inventories are described in sections 2.2 and 2.4, respectively.

2.2. Heterogeneous Reactions

[11] As in *Liao et al.* [2004], hydrolysis of N_2O_5 on surfaces of sulfate, nitrate, ammonium, organic carbon, sea salt, and mineral dust aerosols is considered, but the uptake coefficient $\gamma(N_2O_5)$ has been updated, following the treatment in *Evans and Jacob* [2005]. Instead of using a single $\gamma(N_2O_5)$ of 0.1 for all aerosol types, $\gamma(N_2O_5)$ is taken to depend on aerosol type, relative humidity (RH), and temperature. The relative humidity dependence of $\gamma(N_2O_5)$ on sulfate/nitrate/ammonium aerosol is based on the work of *Kane et al.* [2001], and the temperature dependence is based on the work of *Hallquist et al.* [2003]. $\gamma(N_2O_5)$ on sulfate/nitrate/ammonium aerosols as a function of temperature is defined as a log function fitted to the data presented in *Hallquist et al.* [2003]:

$$\gamma(N_2O_5) = 10^{\beta(T)} \times \left(C_1 + C_2 \times RH + C_3 \times RH^2 + C_4 \times RH^3\right) \quad (1)$$

where RH is relative humidity expressed as a percentage, and T is temperature. $\beta(T) = -4 \times 10^{-2} \times (T - 294)$ when $T \geq 282$K and $\beta(T) = 0.48$ when $T < 282$K. C_1, C_2, C_3, and C_4 are constants whose values are 2.79×10^{-4}, 1.30×10^{-4}, -3.43×10^{-6}, and 7.52×10^{-8}, respectively [*Kane et al.*, 2001]. $\gamma(N_2O_5)$ on OC is based on a fitting of data presented in *Thornton et al.* [2003]; that on sea salt is based on the recommendation of *Atkinson et al.* [2004]. $\gamma(N_2O_5)$ on mineral dust is taken from *Bauer et al.* [2004]. These updated values in $\gamma(N_2O_5)$ lead to an annual and global average $\gamma(N_2O_5)$ of 0.025, when $\gamma(N_2O_5)$ for a grid box is calculated over all aerosol components and weighted by the relative contribution of each component to the total aerosol surface area. Irreversible absorption of NO_3, NO_2, and HO_2 on wetted surfaces of $SO_4^{2-}/NO_3^-/NH_4^+/NaCl/H_2O$, OC, sea salt, and mineral dust is accounted for; these aerosols are considered to be wet when RH $\geq$ 50%. The uptake coefficients used to calculate the first-order loss rate of gas-phase species on aerosol surfaces are summarized in Table 1.

[12] We also consider the uptake of SO_2 by sea salt aerosol. SO_2 is absorbed into water associated with sea salt as determined by its Henry's law constant, and then oxidized by H_2O_2 and O_3 to form non-sea-salt sulfate. The change in SO_2 concentration by scavenging and oxidation loss in sea salt particles is calculated as in *Liao et al.* [2004]. On sea salt particles, $\gamma(SO_2)$ is assumed to be 0.05 for RH >

50% and 0.005 when RH < 50% [*Song and Carmichael*, 2001].

[13] The importance of heterogeneous reactions on mineral dust aerosol has been established by laboratory, field, and modeling studies [*Fenter et al.*, 1995; *Dentener et al.*, 1996; *Galy-Lacaux and Modi*, 1998; *Tabazadeh et al.*, 1998; *Song and Carmichael*, 2001; *Galy-Lacaux et al.*, 2001; *Goodman et al.*, 2000, 2001; *Underwood et al.*, 2001; *Hanisch and Crowley*, 2001, 2003; *Bauer et al.*, 2004]. While mineral dust aerosol has been shown to take up SO_2, HNO_3, and O_3, heterogeneous reactions on dust are highly uncertain. In the present study we use $\gamma(HNO_3)$ of 0.1 and $\gamma(O_3)$ of 1×10^{-5} based on *Bauer et al.* [2004], who simulated uptake of HNO_3 and O_3 by mineral dust and found close agreement between predicted and measured concentrations of HNO_3 throughout the dust events observed during the MINATROC field campaign. Uptake coefficient for SO_2 on mineral dust is taken from the work of *Dentener et al.* [1996].

2.3. Radiative Forcing by Tropospheric O_3 and Aerosols

[14] Radiative forcing calculations are performed on-line within the GCM every 5 hours. We focus on anthropogenic forcings by O_3 and aerosols in this work, so we calculate the shortwave forcing by O_3, sulfate, nitrate, black carbon, organic carbon, as well as the longwave radiative forcing by O_3. Aerosol radiative forcing by each of above aerosol species, as well as the total forcing by all those aerosols will be examined.

[15] Aerosol optical properties (extinction cross section, single-scattering albedo, and asymmetry parameter) are calculated by Mie theory based on wavelength-dependent refractive indices and aerosol size distributions. The assumptions and parameters used for the calculations of aerosol optical properties are given in *Liao et al.* [2004]. Water uptake by each of sulfate and nitrate aerosols is determined by the aerosol thermodynamic equilibrium module, ISORROPIA, which uses the Zdanovskii-Stokes-Robinson (ZSR) correlation [*Robinson and Stokes*, 1965] to calculate the water content of the aerosols. Water uptake by organic carbon aerosol follows the treatment in the work of *Chung and Seinfeld* [2002]. Black carbon is assumed to have no water uptake. In calculating radiative forcing by mixed sulfate, nitrate, BC, and OC aerosols, we consider the two limiting cases that these aerosols are either internally or externally mixed. The refractive indices of the internal mixture are calculated by volume-weighting the refractive indices of each aerosol species and water.

[16] The present-day optical depths and single-scattering albedos predicted by this model have been evaluated by comparisons with measurements in *Liao et al.* [2004]. Most predicted monthly-average aerosol optical depths agree with AERONET measured values within a factor of two, but aerosol optical depths over biomass burning areas are underpredicted. Agreement is generally good between modeled single-scattering albedos and ground measured and AERONET retrieved values, except that single-scattering albedos calculated based on currently available dust refractive indices tend to be lower than recently measured values over dust regions. Such discrepancies between predicted and measured single-scattering albedos over dust regions have no impact on the results presented here, since we focus on anthropogenic aerosol forcings.

2.4. Emission Scenarios

[17] To identify the anthropogenic forcing by tropospheric O_3 and aerosols, we perform several simulations for preindustrial (roughly corresponding to 1800), present-day (year 2000), and the year 2100. Emissions specified for these simulations are summarized in Table 2. The present-day emission inventories for gas-phase species and aerosols are based on the values used in *Liao et al.* [2003, 2004], with several updates on sulfur, DMS and NH_3 emissions. Instead of using the Global Emissions Inventory Activity (GEIA) sulfur emissions [*Benkovitz et al.*, 1996] that are representative of 1985 emissions, we prescribe sulfur emissions for the present-day based on the IPCC SRES A2 emissions scenario, which leads to a change in anthropogenic sulfur emission from 66.6 Tg S yr^{-1} to 69 Tg S yr^{-1}. Following the treatment in *Adams et al.* [2001], anthropogenic NH_3 emissions for 2000 are obtained by scaling the values used in *Liao et al.* [2003, 2004] with N_2O emissions prescribed in the IPCC SRES A2 scenario, because the values used in *Liao et al.* [2003, 2004] were based on GEIA emission inventory of *Bouwman et al.* [1997] that represents emissions for the year 1990. While DMS emissions in *Liao et al.* [2003, 2004] were from *Koch et al.* [1999] with a yearly emission of 10.7 Tg S yr^{-1}, the year 2000 DMS emissions are now prescribed according to IPCC SRES A2 emissions scenario with an annual emission of 25.3 Tg S yr^{-1}. Global natural emissions of DMS, volcanic SO_2, NH_3 from the oceans, undisturbed soils, and wild animals, monoterpene and other reactive volatile organic compounds (ORVOC) for SOA simulation, mineral dust, sea salt, NO_x from soil and lightning, as well as isoprene, $\geq C_3$ alkenes, and acetone from vegetation are assumed unchanged in the 1800, 2000, and 2100 simulations. The cross-tropopause flux of O_3 is also assumed to be the same in all the simulations presented in the work. Methane concentrations are set throughout the troposphere at 0.7, 1.7, and 4.3 ppm in atmospheres of 1800, 2000, and 2100, respectively [*Mickley et al.*, 2004; *Gauss et al.*, 2003].

[18] Preindustrial biomass burning emissions of NO_x, CO, and those of $\geq C_3$ alkenes, acetone, SO_2, NH_3, primary organic carbon, and BC are reduced to 10% of their present-day values. Emissions of NH_3 from livestock, crops, humans, and pets are assumed to be proportional to human population, which was taken to be 20% of the present-day value in 1800 [*Adams et al.*, 2001].

[19] Anthropogenic 2100 sulfur emissions are prescribed according to the IPCC SRES A2 emissions scenario [*Nakicenovic et al.*, 2000]. Anthropogenic NH_3 emissions in the year 2100 are scaled based on N_2O projections. For the 2100 emissions of primary organic carbon and BC, the emissions used in *Liao et al.* [2003, 2004] are scaled with the CO emissions in the IPCC SRES A2 scenario [*IPCC*, 2001, chapter 5]. Year 2100 emissions of NO_x, CO, and NMHC are calculated as the present-day emissions plus the delta emission (2100−2000) provided by the IPCC SRES A2 scenario [*Gauss et al.*, 2003].

2.5. Sensitivity Runs

[20] The focus of this work is to explore the effects of chemistry-aerosol interactions on estimates of anthropogenic

Table 2. Global Annual Emissions for the Years of 1800, 2000, and 2100

Species	Scenario: Preindustrial 1800	Present-Day 2000	IPCC SRES A2 2100
NO_x, Tg N yr^{-1}			
Fossil fuel combustion	0.0	20	96
Biomass burning	1.1	11	11
Soil (natural)	3.9	3.9	3.9
Soil (fertilizer)	0.0	0.5	0.5
Lightning	3.5	3.5	3.5
Aircraft	0.0	0.5	2.2
Stratosphere[a]	0.1	0.1	0.1
Total	8.6	40[b]	117
CO, Tg CO yr^{-1}			
Fossil fuel combustion	0.0	390	1858
Wood fuel combustion	0.0	130	130
Biomass burning	51	510	510
Total	51	1030[b]	2498
Isoprene, Tg C yr^{-1}			
Vegetation	550	550[b]	550
Ethane, Tg C yr^{-1}			
Industrial	0.0	6.2	97.7
Biomass burning	0.2	2.4	2.4
Total	0.2	8.6[b]	100.1
Propane,[d] Tg C yr^{-1}			
Industral	0.0	6.7	28.1
$\geq C_4$ alkanes, Tg C yr^{-1}			
Industrial	0.0	30.1[b]	60.5
$\geq C_3$ alkenes, Tg C yr^{-1}			
Industrial	0.0	10	29
Biogenic sources	16	16	16
Biomass burning	1.2	12	12
Total	17.2	38[b]	57
Acetone, Tg C yr^{-1}			
Biomass burning	0.9	9	9
Biogenic sources	14	14	14
Total	14.9	23[b]	23
SO_2, Tg S yr^{-1}			
GEIA industrial emissions	0.0	69	60.3
Biomass burning	0.2	2.3	2.3
Volcanoes (noneruptive)	3.5	3.5	3.5
Total	3.7	74.8	66.1
DMS, Tg S yr^{-1}			
Oceanic source	25.3	25.3	25.3
NH_3, Tg N yr^{-1}			
Agricultural	6.8	37.4	88.8
Natural	10.7	10.7	10.7
Biomass burning	0.6	6.4	15.3
Other	0.6	3.1	7.4
Total	18.7[c]	57.6[c]	122.2[c]
Hydrocarbon for SOA, Tg C yr^{-1}			
Vegetation	172.8[e]	172.8[e]	172.8[e]
POA, Tg OM yr^{-1}			
Biomass burning	5.4	54	
Fossil fuel	0.0	28.2	
Total	5.4	82.2[f]	189.5[h]
BC, Tg C yr^{-1}			
Biomass burning	0.56	5.6	
Fossil fuel	0.0	6.6	
Total	0.56	12[f,g]	28.8[h]

[a]Downward transport of NO_x across the tropopause. This transport also supplies 0.38 Tg N yr^{-1} of HNO_3 globally.
[b]*Mickley et al.* [1999].
[c]*Bouwman et al.* [1997]; *Adams et al.* [2001].
[d]Included in the model as a direct emission of acetone; the yield of acetone from oxidation of propane is specified as 80%.
[e]*Griffin et al.* [1999a].
[f]*Liousse et al.* [1996].
[g]*Penner et al.* [1998].
[h]Scaled to projected changes in CO.

direct radiative forcing of tropospheric O_3 and aerosols. Baseline simulations are performed for each time period with fully coupled gas-phase chemistry and aerosols, including the following heterogeneous reactions: (1) heterogeneous reactions of N_2O_5, NO_3, NO_2, and HO_2 on aerosols; (2) uptake of SO_2 by sea salt; (3) uptake of SO_2, HNO_3 and O_3 by mineral dust. The effects of all aerosol classes (sulfate/nitrate/ammonium/sea salt/water, black carbon, primary organic carbon, secondary organic carbon, sea salt, and mineral dust aerosols) on photolysis rates are included in all simulations presented in this work. All simulations are conducted for an 18-month period, with the first 6 months ignored for spin-up.

[21] In addition to these baseline simulations, three sensitivity simulations are performed for each time period to identify the effects of different heterogeneous reactions. First, for each time period a sensitivity run is performed in the absence of all heterogeneous reactions (hereafter referred to as NOHET). The second sensitivity simulation (hereafter referred to as HETNODUST), for each of the three time periods, retains heterogeneous reactions of N_2O_5, NO_3, NO_2, and HO_2 on aerosols and the uptake of SO_2 by sea salt, but removes the uptake of SO_2, HNO_3 and O_3 by mineral dust. Finally, we perform a sensitivity study (hereafter referred to as HETDUST) for each period considering the uptake of SO_2, HNO_3, and O_3 by mineral dust only. HETNODUST and HETDUST are designed to separate the effects of the relatively less uncertain heterogeneous reactions from the highly uncertain reactions on mineral dust aerosol. The heterogeneous reactions that are considered in the baseline and each of the sensitivity simulations are shown in Table 1.

3. Predicted Tropospheric O_3 and Aerosol Burdens in Preindustrial, Present-Day, and Future Scenarios

[22] This section presents predicted concentrations of O_3, SO_4^{2-}, NO_3^-, black carbon, primary organic carbon, and secondary organic carbon aerosols that contribute to anthropogenic radiative forcing. Since concentrations of O_3, SO_4^{2-}, and NO_3^- depend on chemistry-aerosol coupling, we discuss the effects of heterogeneous reactions by comparing results from the baseline simulations to those from the sensitivity studies. We also show how chemistry-aerosol coupling influences predicted total aerosol mass and aerosol water content.

3.1. Tropospheric O_3

[23] Surface-layer O_3 concentrations from the baseline simulations of the three time periods are shown in Figure 1 for January and July. Predicted preindustrial O_3 concentrations are about 15–20 ppbv in the winter hemisphere, while concentrations are mostly in the range of 5–10 ppbv in the summer hemisphere, because of the larger amount of O_3 transported from the stratosphere in winter and the enhanced chemical loss of O_3 in summer. High concentrations in mountain regions such as the Himalayas, Greenland, and the Rocky Mountains are a result of stratospheric transport. Ozone concentrations of 20–30 ppbv are also predicted over biomass burning regions in tropics. In the present-day and 2100 simulations, predicted O_3 concentration fields over

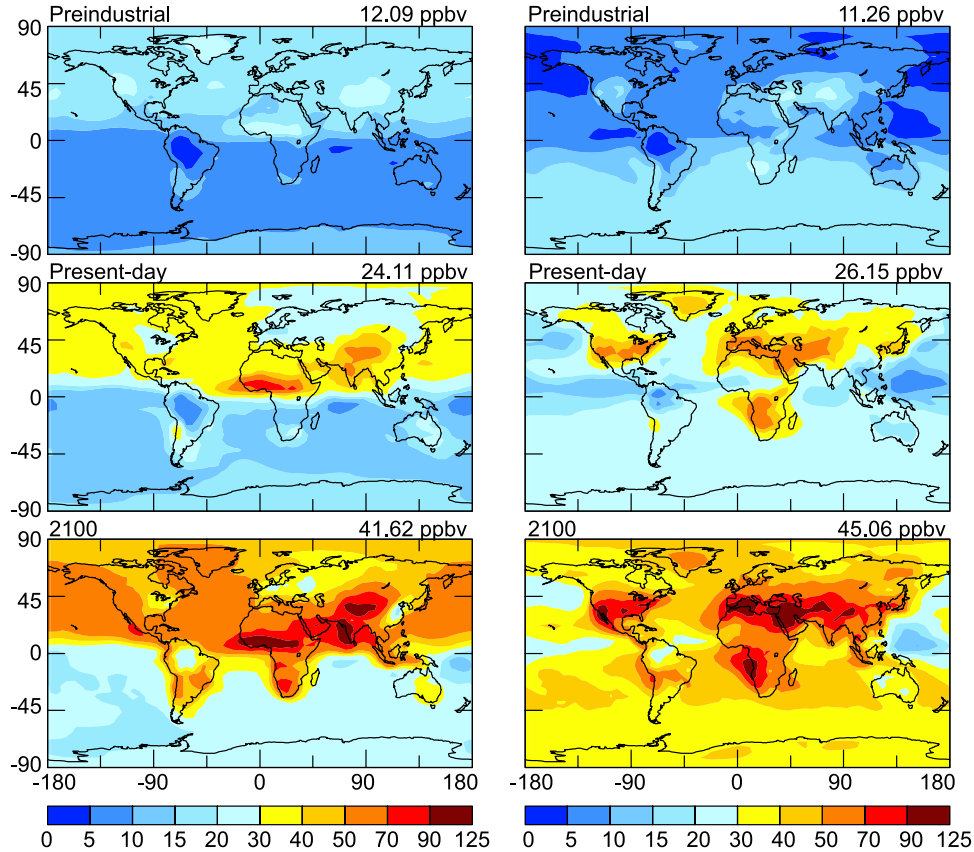

Figure 1. Surface layer ozone mixing ratios (ppbv) in January (left column) and July (right column) predicted from the baseline simulations for preindustrial, present-day, and year 2100. All heterogeneous reactions listed in Table 1 are included in baseline simulations. Above each panel, the time period of the simulation and the global mean mixing ratio are indicated.

North America and Europe in July reach values as high as 70 ppbv under present-day conditions and 116 ppbv in the year 2100.

[24] Predicted global and annual O_3 burdens from the baseline simulations are 190.0, 318.5, and 518.6 Tg for the preindustrial, present-day, and 2100 scenarios (Table 3), respectively. A 68% increase in O_3 burden is predicted from the preindustrial time to present-day, which agrees closely with the approximate 65% increase reported by *Wang and Jacob* [1998] and *Lelieveld and Van Dorland* [1995]. For O_3 increase from present-day to year 2100, *Gauss et al.* [2003], based on 11 different chemical transport models, reported that the predicted annual and global mean increase in tropospheric O_3 ranged from 11.4 to 20.5 DU when IPCC SRES A2 was used. Our predicted O_3 change from present-day to year 2100, when converted to DU, is 18.3 DU, which is near the higher end of the changes reported in *Gauss et al.* [2003].

[25] As described in section 2.5, three sensitivity studies, NOHET, HETNODUST, and HETDUST, investigate the effects of all heterogeneous reactions, nondust heterogeneous reactions, and mineral dust uptake, respectively. The percentage differences between the surface O_3 concentrations from the baseline (with all heterogeneous reactions), HETNODUST, and HETDUST simulations and those from the NOHET simulation are shown in Figure 2 for the three time periods. Because preindustrial concentrations of sul-

Table 3. Global and Annual Average Burdens Obtained From the Baseline and Sensitivity Simulations[a]

	NOHET	HETNODUST	HETDUST	Baseline
		Preindustrial		
O_3	202.0	201.4	190.7	190.0
SO_4^{2-}	0.61	0.42	0.47	0.32
NO_3^-	0.30	0.30	0.18	0.18
BC	0.011	0.011	0.011	0.011
POA	0.095	0.096	0.096	0.096
SOA	0.22	0.22	0.23	0.23
Aerosol H_2O	2.40	2.17	1.81	1.67
		Present-Day		
O_3	356.4	332.3	343.6	318.5
SO_4^{2-}	2.14	1.71	1.75	1.40
NO_3^-	0.49	0.47	0.48	0.48
BC	0.23	0.23	0.23	0.23
POA	1.27	1.27	1.27	1.27
SOA	0.32	0.32	0.32	0.33
Aerosol H_2O	8.93	8.67	8.04	7.86
		Year 2100		
O_3	616.5	530.3	602.8	518.6
SO_4^{2-}	1.98	1.60	1.70	1.37
NO_3^-	2.36	2.22	2.16	1.97
BC	0.54	0.54	0.54	0.54
POA	2.94	2.94	2.94	2.94
SOA	0.37	0.37	0.37	0.37
Aerosol H_2O	14.8	15.6	13.5	14.4

[a]Units are in Tg.

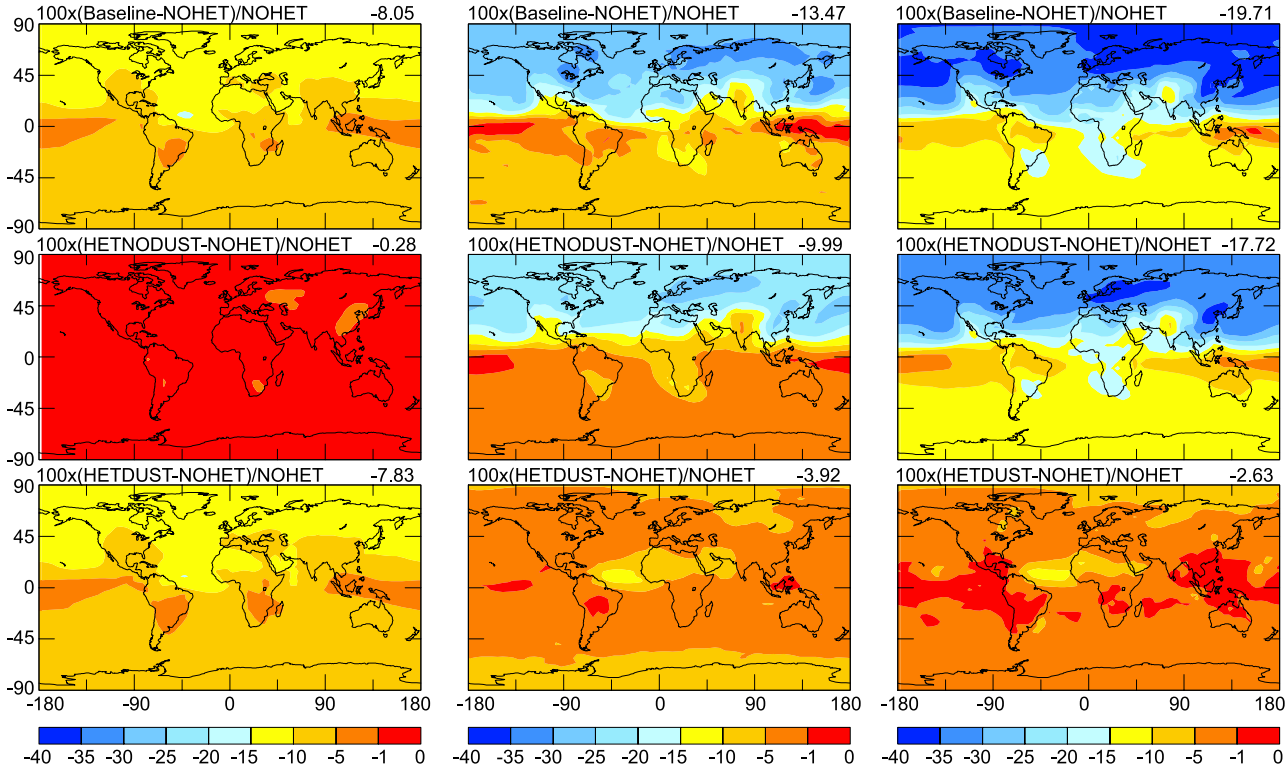

Figure 2. Percentage differences in annual mean surface layer ozone concentrations resulting from heterogeneous reactions for preindustrial (left column), present-day (middle column), and 2100 (right column) atmospheres. Top, middle, and bottom panels show effects of all heterogeneous reactions [100 × (Baseline − NOHET)/NOHET], effects of nondust heterogeneous reactions [100 × (HETNODUST − NOHET)/NOHET], and effects of dust-associated heterogeneous reactions [100 × (HETDUST − NOHET)/NOHET], respectively.

fate, nitrate, and carbonaceous aerosols are low, the effects of heterogeneous reactions of N_2O_5, NO_3, NO_2, and HO_2 on O_3 are negligible, which produce just a 0.28% reduction in surface O_3 concentration on an annual and global mean basis. Since concentrations of mineral dust are assumed to be the same for the three time periods, mineral dust uptake of HNO_3 and O_3 is predicted to play a more important role in determining preindustrial O_3 concentrations. Reduction of O_3 by dust affects the entire globe because of the long chemical lifetime (about 4 weeks) of O_3 [*Mickley et al.*, 1999; *Liao et al.*, 2003]; preindustrial O_3 concentrations are generally reduced by 10–15% in the NH and 5–10% in the SH, as compared with the O_3 concentrations predicted without heterogeneous reactions. With the increase of anthropogenic aerosol burdens from the preindustrial time, nondust heterogeneous reactions assume greater importance than mineral dust uptake in the present-day and year 2100 atmospheres. Compared with the O_3 concentrations from the NOHET simulations, the annual and global mean changes in surface O_3 concentrations caused by the nondust heterogeneous reactions and the dust uptake are −10.0% and −3.9% in present-day, and −17.7% and −2.6% in year 2100, respectively. Nondust heterogeneous reactions mainly influence O_3 concentrations in the Northern Hemisphere, with surface O_3 concentrations at NH mid to high latitudes reduced by 25–35% in present-day and 30–41% in year 2100, whereas the mineral dust uptake is predicted to produce the largest O_3 reductions of 10–15% in the downwind of the Sahara Desert in both the present-day and year 2100.

[26] The effect of mineral dust on O_3 has been reported in a number of global studies for the present-day atmosphere. *Bian and Zender* [2003], using $\gamma(HNO_3) = 0.001$ and $\gamma(O_3) = 5 \times 10^{-5}$, predicted a reduction of O_3 of about 8.5% near African dust sources. *Bauer et al.* [2004] used $\gamma(HNO_3) = 0.1$ and $\gamma(O_3) = 10^{-5}$ and reported a 20–25% O_3 reduction near and downwind of the Sahara. *Tie et al.* [2005] used the same uptake coefficients as those in *Bauer et al.* [2004] and predicted a maximum O_3 reduction of about 20% near the Sahara. The differences between these predictions result from differences in predicted dust and O_3 burdens, as well as the assumed dust surface area.

3.2. Sulfate

[27] Predicted annual mean surface-layer concentrations and tropospheric column burdens of sulfate aerosol from the baseline simulations are shown in Figure 3 for the three time periods. Preindustrial sulfate mixing ratios are predicted to be generally below 100 pptv globally. In the absence of anthropogenic emissions, preindustrial sulfate formation depends on DMS emissions over the oceans; predicted surface sulfate concentrations are the highest around 60° in both hemispheres. Present-day and 2100 sulfate concentrations peak over industrialized Europe, eastern China, and United States, with surface mixing ratios exceeding 1 ppbv and column burdens in the range of 5–20 mg m^{-2}. With

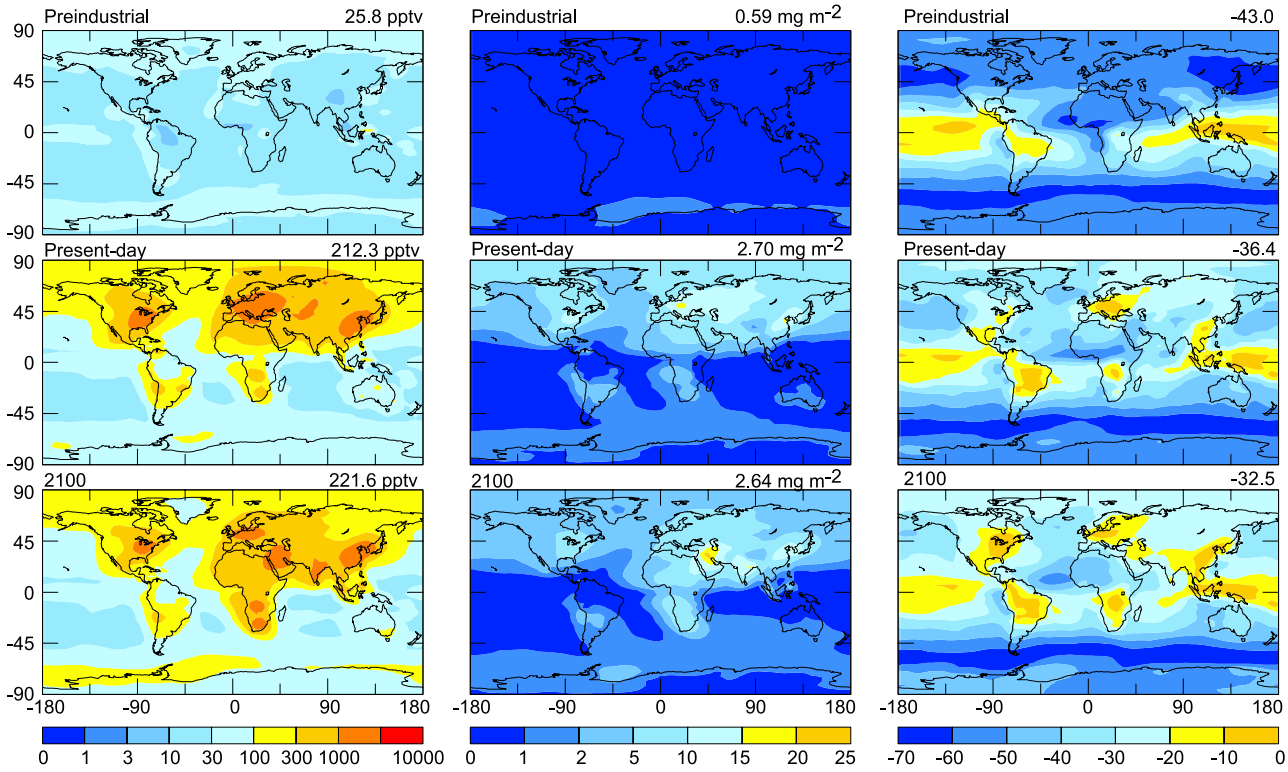

Figure 3. Predicted annual mean surface layer sulfate mixing ratios (pptv) (left column) and sulfate tropospheric column loadings (mg m^{-2}) (middle column) for preindustrial, present-day, and year 2100 baseline simulations. Baseline simulations consider all heterogeneous reactions listed in Table 1. The percentage differences ((Baseline-NOHET) × 100/NOHET) in sulfate column burdens between the baseline and NOHET simulations for the three time periods are shown in the right column. Above each panel, the time period of the simulation and the global mean value are indicated.

anthropogenic sulfate emissions in the present-day atmosphere being close to those in year 2100 in SRES A2, sulfate concentrations and distributions are predicted to show little change from the present-day to year 2100.

[28] Heterogeneous reactions that have direct impact on sulfate concentrations are sea salt uptake of SO_2 and mineral dust uptake of SO_2. The percentage differences ((Baseline-NOHET) × 100/NOHET) in sulfate column burdens between the baseline and NOHET simulations are also shown in Figure 3. For all the three time periods, sea salt uptake is predicted to reduce sulfate column burdens by about 65% near 60°S where emissions of DMS and sea salt are both very high. Sea salt uptake is also important over oceans around 45°N. With Asian dust uptake of SO_2 occurring at about the same latitudes, sulfate column burdens over northeast Asia and the North Pacific Ocean are predicted to be reduced by about 60% in the preindustrial atmosphere. Mineral dust uptake of SO_2 is predicted to reduce sulfate column burdens by 50–70% near or downwind of the Sahara for all the three periods. Compared with the NOHET simulation, the present-day and year 2100 sulfate column burdens over the industrialized areas and biomass burning regions are reduced by about 10% in the presence of heterogeneous reactions, which is mainly a result of the reduction (of O_3 (see Figure 2) and OH [*Dentener and Crutzen*, 1993] from the uptake of NO_3, NO_2, and HO_2 by wet aerosols, leading to the reduction in sulfate formation from both gas-phase and in-cloud reactions.

3.3. Nitrate

[29] Nitrate aerosol forms from the partitioning of HNO_3 between gas and aerosol phases. Gas-phase HNO_3 in the atmosphere is produced mainly by the reaction of NO_2 with OH and at night by hydrolysis of N_2O_5 on aerosol surfaces. Global distributions of annual mean nitrate aerosol concentrations at the surface layer from the baseline and the HETNODUST, HETDUST, and NOHET sensitivity simulations are presented in Figure 4 for the three time periods. Preindustrial NO_x emissions arise from natural sources such as biomass burning, vegetation, soil, lighting, and cross-tropopause transport. The highest preindustrial nitrate concentrations are predicted in the SH as a result of biomass burning. As expected, present-day and year 2100 nitrate concentrations are the highest over Europe, Eastern China, and North America; baseline nitrate mixing ratios in these areas exceed 1 ppbv in the present-day and 3 ppbv in year 2100. With sulfur emissions in year 2100 slightly lower than the present-day values, and emissions of NH_3 and NO_x predicted to increase significantly from present-day to year 2100 (Table 2), ammonium nitrate formation is favored in year 2100. On an annual mean basis, the ratio of the global burden of gas-phase HNO_3 to that of nondust nitrate is predicted to be 2.7 in present-day and 1.1 in year 2100.

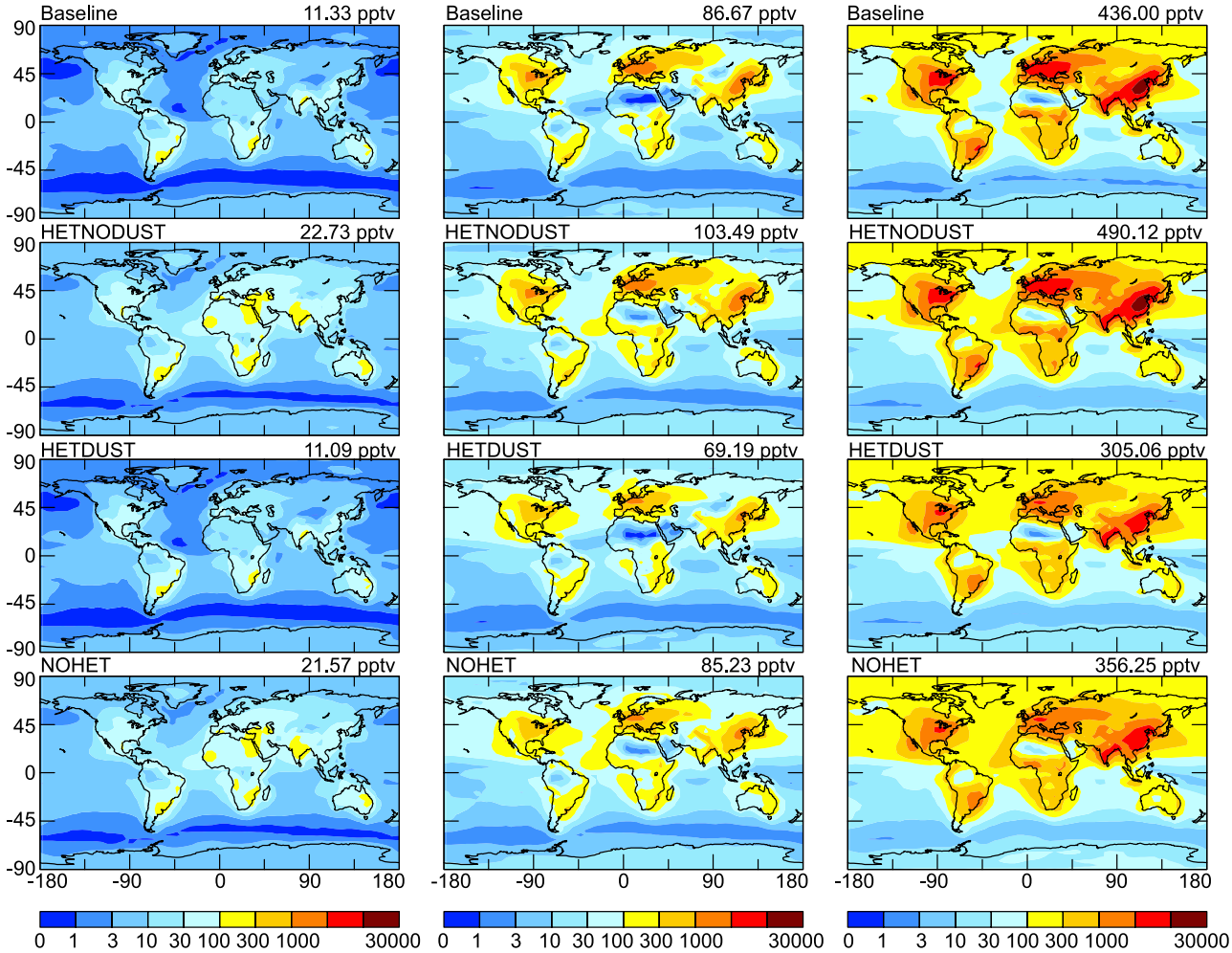

Figure 4. Predicted annual mean nitrate aerosol mixing ratios (pptv) at the surface layer from the baseline (with all heterogeneous reactions listed in Table 1) and the HETNODUST (with nondust heterogeneous reactions only), HETDUST (with dust-associated heterogeneous reactions only), and NOHET (with all reactions listed in Table 1 removed) sensitivity simulations for preindustrial (left column), present-day (middle column), and 2100 (right column). Above each panel, the particular simulation and the global mean value are indicated.

[30] Whereas hydrolysis of N_2O_5 increases HNO_3, reactions of NO_3, NO_2 and HO_2 on aerosols reduce HNO_3 concentrations because of the reduction of HO_x (HO_2 + OH). Compared with the NOHET simulation, absorption of NO_x by aerosols reduces O_3 concentrations (section 3.1), leading to lower OH concentrations from $O_3 + h\nu \rightarrow O(^1D) + O_2$ and $O(^1D) + H_2O \rightarrow 2OH$ reactions. In addition, the absorption of HO_2 by aerosols reduces OH formation via $HO_2 + O_3 \rightarrow OH + 2O_2$ and $HO_2 + NO \rightarrow NO_2 + OH$ reactions. Present-day and 2100 surface layer OH concentrations over industrial areas are predicted to be reduced by about 60% in the presence of heterogeneous reactions (not shown), resulting in lower HNO_3 production from the reaction of NO_2 with OH. In summary, heterogeneous reactions considered in the HETNODUST simulation can either increase or reduce HNO_3 concentrations depending on the competition between the hydrolysis of N_2O_5 and the absorption of NO_3, NO_2 and HO_2 by wet aerosols. Compared to the NOHET simulations, the overall effect of reactions of N_2O_5, NO_3, NO_2, and HO_2 on aerosol surfaces is to increase the global and annual mean nitrate concentration at the surface layer by 5%, 21%, and 38% in the preindustrial, present-day, and year 2100, respectively (Figure 4). Mineral dust uptake of HNO_3 also influences nitrate concentrations significantly; the annual and global mean surface layer nitrate concentration from the HETDUST simulation is 49% lower in the preindustrial atmosphere, 19% lower in the present-day, and 14% lower in year 2100 as compared to the value from the NOHET simulation.

[31] Figure 5 shows the ratios of annual mean column burdens of nitrate from the baseline, HETNODUST, and HETDUST simulations to those from the NOHET simulation for the three time periods. The effects of nondust heterogeneous reactions are not important in the preindustrial time; compared with the NOHET simulation, nitrate column burdens in the HETNODUST case are slightly lower in the high latitudes of the NH, resulting from the NO_x reduction by aerosols, and show small increases between −90°S and +45°N, which can be explained by the increased ammonium nitrate formation because of sea

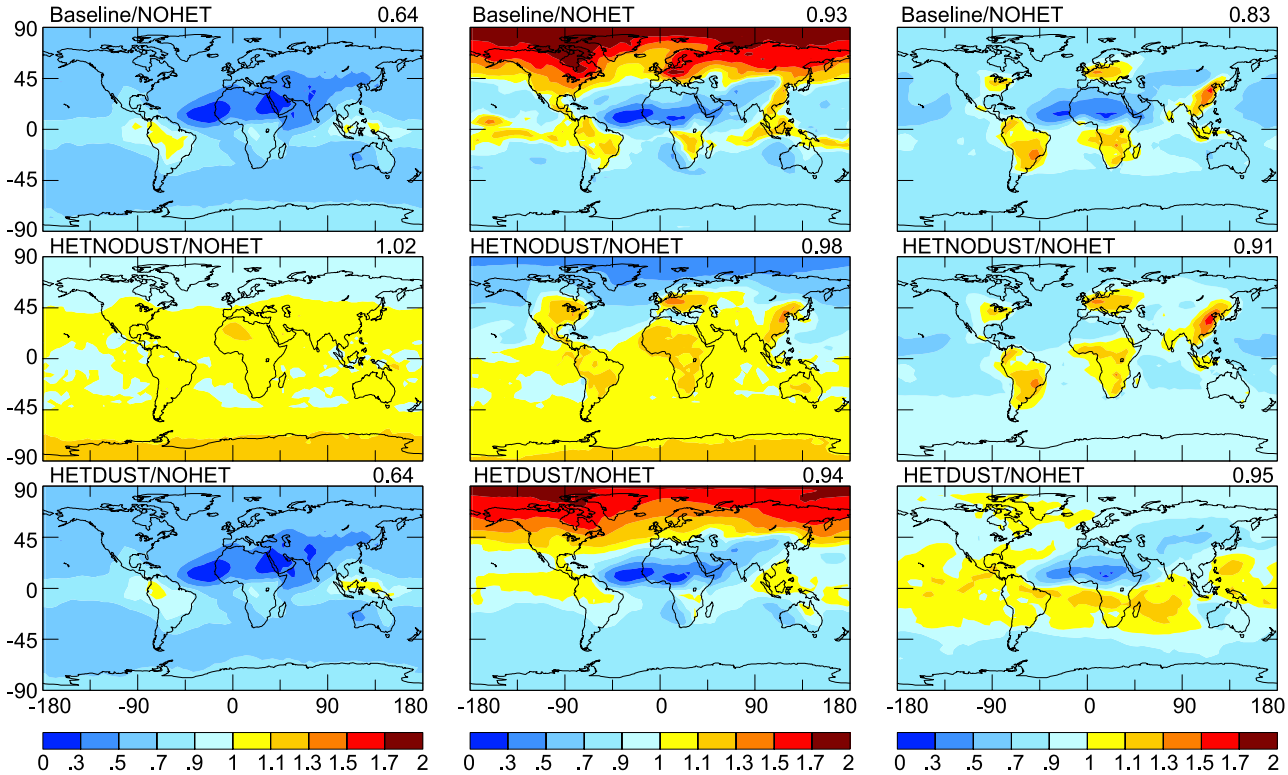

Figure 5. Ratios of annual mean column burdens of nitrate from the baseline, HETNODUST, and HETDUST simulations to those from the NOHET simulation for the preindustrial (left column), the present-day (middle column), and 2100 (right column). Baseline, HETNODUST, HETDUST, and NOHET simulations consider all heterogeneous reactions, nondust heterogeneous reactions, dust-associated heterogeneous reactions, and no heterogeneous reactions, respectively.

salt uptake of SO_2. Such a pattern of changes in nitrate column burdens by nondust heterogeneous reactions holds in the present-day atmosphere, except nitrate column burdens increase by 30–50% over Europe, Eastern United States, and Eastern China, where hydrolysis of N_2O_5 dominates. In year 2100, nondust heterogeneous reactions are predicted to increase nitrate column burdens over populated and biomass burning regions but reduce burdens elsewhere. Burdens over the Eastern United States, Europe, and Eastern China are predicted to increase by 10–30%, 30–50%, and 50–70%, respectively, as compared with the year 2100 NOHET simulation.

[32] Mineral dust significantly reduces nitrate burdens near the Sahara Desert, with the highest reduction of about 85% in preindustrial and present-day atmospheres, and of 70% in year 2100. These large reductions agree with the predictions of *Dentener et al.* [1996]. A unique feature of the effect of dust uptake in the present-day is that nitrate burdens actually are predicted to increase in the high latitudes in the NH. This can be explained by dust uptake of SO_2, which leads to less sulfate in the upper troposphere and promotion of ammonium nitrate formation.

[33] Since predicted nitrate concentration is closely related to the formation of gas-phase HNO_3, we show in Table 4 the annual HNO_3 budget for the baseline and the NOHET simulations in present-day and year 2100. There are 23 gas-phase reactions that produce HNO_3 and 2 reactions that remove it. The most important sources of HNO_3 are the reaction of NO_2 with OH (reaction (R1) in Table 4), reactions of NO_2 and N_2O_5 on aerosols (reactions (R21) and (R23)), reaction of DMS with NO_3 (reaction (R20)), and reactions of NO with RO_2 radicals from isoprene (reactions (R4) and (R10)). The hydrolysis of N_2O_5 accounts for 26.5% and 35.8% of HNO_3 production in present-day and year 2100, respectively, in the baseline simulations, which explains the increased burdens of nitrate aerosol in the industrialized regions in the presence of nondust heterogeneous reactions. The NO_2 + OH reaction accounts for 36.5 % and 36.8% of HNO_3 production in present-day and year 2100, respectively, in the baseline simulations, while it contributes to 55.5% of present-day HNO_3 production and 61.8% of year 2100 production in the absence of heterogeneous reactions, which can be explained by the higher OH concentrations in the absence of heterogeneous reactions. Global mean surface layer OH concentrations predicted in year 2100 NOHET simulation are higher than those predicted in present-day NOHET simulation by 11% in January and 18% in July, which also helps to explain the large contribution from the NO_2 + OH reaction in year 2100 when no heterogeneous reactions are considered.

3.4. Carbonaceous Aerosols

[34] Figure 6 presents the predicted annual mean BC, POA, and SOA surface-layer concentrations for the three time periods. Preindustrial carbonaceous aerosols are predicted to be the highest over the biomass burning areas in South America and Africa. One interesting feature of the predicted preindustrial carbonaceous aerosols is that,

Table 4. Annual Mean HNO_3 Budget for Present-Day and Year 2100 Simulations[a]

	Present-Day		Year 2100	
	Baseline	NOHET	Baseline	NOHET
Chemical Productions, Tg yr^{-1}	153.5	154.5	464.0	457.3
(R1) $NO_2 + OH + M \rightarrow HNO_3 + M$	36.5%	55.5%	36.8%	61.8%
(R2) $NO_3 + CH_2O \rightarrow HNO_3 + prod.$	1.1%	3.8%	2.2%	8.9%
(R3) $ALD2 + NO_3 \rightarrow HNO_3 + prod.$	0.8%	3.2%	1.8%	6.6%
(R4) $RIO2 + NO \rightarrow HNO_3 + prod.$	9.3%	9.1%	3.9%	3.7%
(R5) $RIO1 + NO \rightarrow HNO_3 + prod.$	0.8%	0.7%	0.4%	0.3%
(R6) $IAO2 + NO \rightarrow 0.08HNO_3 + prod.$	0.3%	0.3%	0.1%	0.1%
(R7) $VRO2 + NO \rightarrow HNO_3 + prod.$	0.9%	0.9%	0.4%	0.4%
(R8) $MRO2 + NO \rightarrow HNO_3 + prod.$	0.6%	0.6%	0.3%	0.2%
(R9) $MVN2 + NO \rightarrow 0.1HNO_3 + prod.$	0.0%	0.1%	0.0%	0.1%
(R10) $INO2 + NO \rightarrow 0.85HNO_3 + prod.$	4.7%	5.8%	2.6%	3.6%
(R11) $ALK4 + NO_3 \rightarrow HNO_3 + prod.$	0.0%	0.4%	0.1%	0.5%
(R12) $RCHO + NO_3 \rightarrow HNO_3 + prod.$	0.1%	0.4%	0.2%	0.7%
(R13) $MEK + NO_3 \rightarrow HNO_3 + prod.$	1.1%	3.3%	0.8%	2.9%
(R14) $INO2 + MO2 \rightarrow 0.425HNO_3 + prod.$	0.6%	0.8%	0.2%	0.3%
(R15) $GLYX + NO_3 \rightarrow HNO_3 + prod.$	0.0%	0.0%	0.0%	0.0%
(R16) $MGLY + NO_3 \rightarrow HNO_3 + prod.$	0.2%	0.8%	0.3%	1.5%
(R17) $MACR + NO_3 \rightarrow HNO_3 + prod.$	0.3%	0.7%	0.2%	0.8%
(R18) $C_2H_6 + NO_3 \rightarrow HNO_3 + prod.$	0.0%	0.0%	0.1%	0.2%
(R19) $INO2 + MCO3 \rightarrow 0.85HNO_3 + prod.$	2.2%	2.8%	1.0%	1.1%
(R20) $DMS + NO_3 \rightarrow HNO_3 + prod.$	7.4%	10.8%	4.1%	6.3%
(R21) $NO_2 + (aerosols) \rightarrow 0.5HNO_3 + prod.$	6.2%	0.0%	8.2%	0.0%
(R22) $NO_3 + (aerosols) \rightarrow HNO_3 + prod.$	0.3%	0.0%	0.4%	0.0%
(R23) $N_2O_5 + (aerosols) \rightarrow 2HNO_3$	26.5%	0.0%	35.8%	0.0%
Total loss, Tg yr^{-1}	153.5	154.5	464.0	457.3
Chem. loss, Tg yr^{-1}	10.7	20.0	24.9	44.6
(R24) $HNO_3 + OH \rightarrow prod.$	34.6%	37.0%	32.9%	36.8%
(R25) $HNO_3 + hv \rightarrow prod.$	65.4%	63.0%	67.1%	63.2%
Dust uptake, Tg yr^{-1}	37.1	0	73.0	0
Loss to nitrate,[b] Tg yr^{-1}	36.9 (105.3−68.4)	46.0 (123.5−77.5)	168.7 (394.4−225.7)	176.1 (470.7−294.6)
Dry deposition, Tg yr^{-1}	27.3	35.6	80.1	97.2
Wet deposition, Tg yr^{-1}	41.5	52.9	117.3	139.4
Burden, Tg	1.30	1.78	2.16	2.98

[a]The numbers for reactions (R1)–(R25) are contributions to chemical production or loss from each reaction. Please see http://www-as.harvard.edu/chemistry/trop/geos/doc/chem_mech/geoschem_mech.pdf for the formula of the species in these reactions and for the rate constants.

[b]The first number in the parentheses is the loss of gas-phase HNO_3 to nitrate formation, and the second number shows the release of gas-phase HNO_3 from nitrate, which are determined by aerosol thermodynamics.

although the global and annual mean concentration of SOA in the surface layer is about one-fifth that of POA, the SOA global burden of 0.22 Tg is 129% higher than the POA burden of 0.096 Tg (Table 3) based on the baseline calculation. This can be explained based on the assumptions about preindustrial emissions of monoterpenes and ORVOCs and about the transport of NO_x and O_3 from the stratosphere; with these values in the preindustrial time being assumed the same as those in the present-day atmosphere, SOA formation in the upper troposphere does not vary significantly from the preindustrial time to the present-day. In fact, as predicted by *Chung and Seinfeld* [2002], SOA concentrations in the upper troposphere are actually slightly higher during the preindustrial time than in the present-day, because the lower POA concentrations near the surface lead to more gas-phase products transported above the surface layer, ultimately condensing to the aerosol phase at higher altitude. As a result, preindustrial SOA concentrations in the upper troposphere are predicted to have been higher than those near the surface, and the predicted SOA global burden exceeds the POA burden.

[35] In the present-day and year 2100, BC and POA concentrations increase significantly over preindustrial values. Present-day BC and POA global burdens are predicted to be 0.23 and 1.27 Tg, respectively, which are close to the BC burden of 0.22 Tg and POA burden of 1.18 Tg obtained by *Chung and Seinfeld* [2002], who used the same emission inventories for carbonaceous aerosols. The present-day SOA burden of 0.32 Tg is higher than that of 0.19 Tg obtained by *Chung and Seinfeld* [2002]. The SOA simulation in *Chung and Seinfeld* [2002] was based on offline OH fields of C. Spivakovsky (personal communication, 1998) and O_3 and NO_3 fields of *Wang and Jacob* [1998] and an earlier version of the GISS GCM II', which predicted that 98% of oxidation of parent hydrocarbons occurs in the lowest two model layers. With 81% of hydrocarbon oxidation predicted to take place in the lowest two model layers in this work, more oxidation occurs in mid to upper troposphere where lower temperature leads to higher SOA yield. The higher POA concentrations predicted in this work also help to explain the higher SOA formation. In year 2100, BC and POA emissions are predicted to be about 2.4 times the present-day values, leading to predicted burdens of 0.54 Tg for BC and of 2.94 Tg for POA. These predictions exceed the OC burden of 2.16 Tg and BC burden of 0.34–0.40 Tg obtained by *Koch* [2001], mainly a result of the different wet and dry deposition schemes between the models.

[36] BC and POA burdens are not affected by gas-phase chemistry, but SOA levels depend on the concentrations of O_3, OH, and NO_3, which themselves are influenced by heterogeneous chemistry. Sensitivity studies (Table 3) show

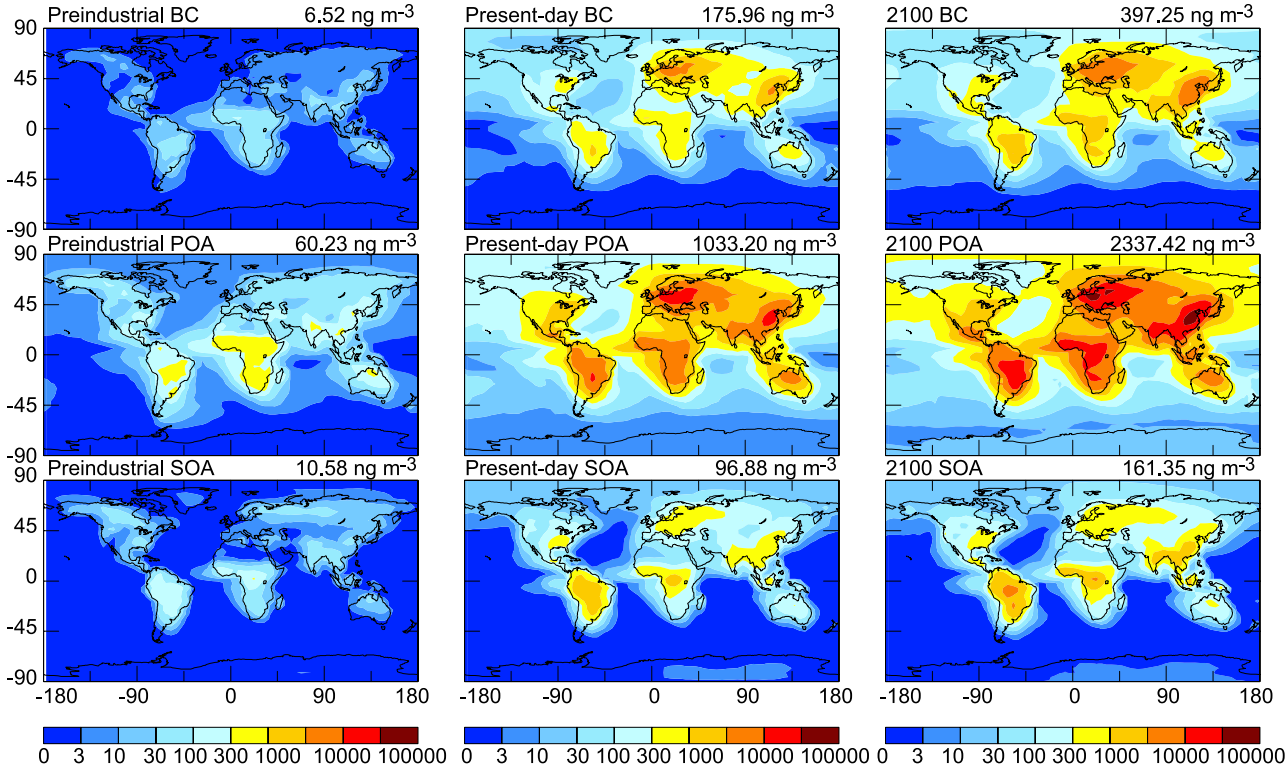

Figure 6. Predicted annual mean BC, POA, and SOA concentrations (ng m^{-3}) at the surface layer for the preindustrial (left column), present-day (middle column), and year 2100 scenarios (right column). Above each panel, the global mean value is indicated.

that heterogeneous reactions have virtually no impact on SOA burdens, because natural monoterpene and other reactive volatile organic carbons are fully oxidized, so the formation of SOA mainly depends on POA available for absorption of SOA.

3.5. Aerosol Mass and Water Content

[37] The dry aerosol mass, the sum of sulfate, nitrate, ammonium, BC, POA, and SOA, at the surface layer from the baseline simulations is shown in Figure 7 for the present-day and year 2100. Under present-day conditions, dry mass concentrations exceeding 15 μg m^{-3} are predicted over Europe, Eastern United States, Eastern China, and over the biomass region in South America. In year 2100, as compared with the present-day values, dry mass concentrations over Europe, South America, and Southern Africa are predicted to double or triple; levels over Eastern United States and Eastern China increase by 60–100% and 200–300%, respectively.

[38] Heterogeneous reactions are predicted to be important in influencing aerosol mass concentrations. Figure 7 also shows the differences between the dry aerosol mass concentrations from the baseline simulations and those obtained in the NOHET simulations. Aerosol mass concentrations predicted in the baseline simulation are higher in Europe, Eastern United States, Eastern China, and biomass burning areas and lower in the rest of the world than those predicted in the NOHET simulation in both the present-day and year 2100. The largest difference of 7.8 μg m^{-3} is predicted over Europe in the present-day, and of 37.9 μg m^{-3} is predicted over Eastern China in year 2100. These large differences between the mass concentrations with or without the chemistry-aerosol coupling arise from the differences in nitrate and ammonium concentrations.

[39] Annual average column burdens (mg m^{-2}) of aerosol water associated with sulfate, nitrate, and OC aerosols are shown in Figure 8 for the present-day and year 2100 baseline simulations. The distributions of aerosol water are similar to those of aerosol mass concentrations shown in Figure 7. The highest column water burden of 230.5 mg m^{-2} is found over Europe in the present-day and of 667.1 mg m^{-2} in year 2100 is located over Eastern China. The percentage differences in aerosol water column burdens between the baseline and the NOHET simulations are also shown in Figure 8. Aerosol water is reduced through sea salt uptake of SO_2 over the oceans and by dust uptake of SO_2 and HNO_3 near dust sources; aerosol water burdens can be reduced by about 60% over the oceans and near dust sources in present-day and year 2100 scenarios. Over the Eastern United States, Europe, and Eastern China, the 20–92% increases in aerosol water burdens in both the present-day and year 2100 atmospheres correspond to the increased ammonium nitrate concentrations. These increases in aerosol water column burdens, together with the changes in nitrate aerosol mass in these industrialized areas (Figure 7), have large impacts on estimates of anthropogenic aerosol forcing there, as will be examined in the next section.

4. Direct Forcing Estimates

[40] Direct and anthropogenic radiative forcing by O_3, individual aerosol species, and all aerosols (sulfate, nitrate,

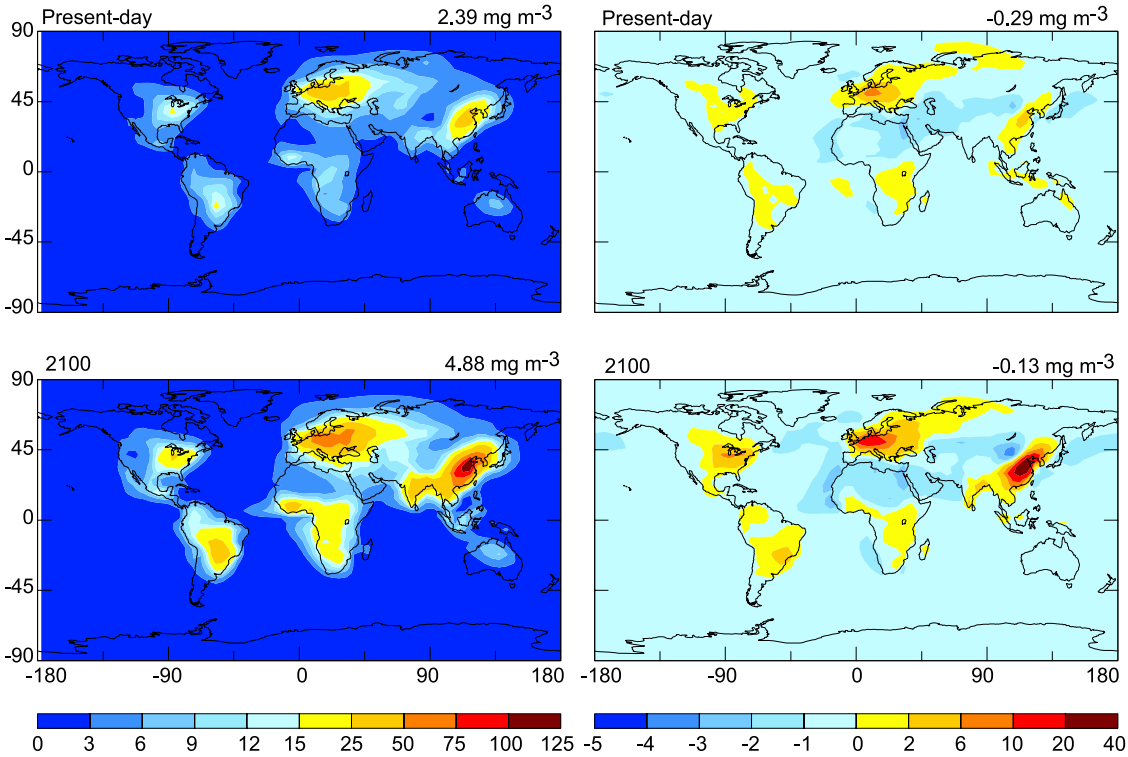

Figure 7. Total dry aerosol mass ($\mu g\ m^{-3}$) of sulfate, nitrate, ammonium, BC, POA, and SOA in the surface layer from the baseline simulations for present-day (top left panel) and year 2100 (bottom left panel). The differences ($\mu g\ m^{-3}$) in the dry aerosol mass concentrations between the baseline and the NOHET simulation (Baseline−NOHET) are shown for present-day (top right panel) and year 2100 (bottom right panel). All the heterogeneous reactions listed in Table 1 are considered in the baseline simulations, whereas all these heterogeneous reactions are removed in the NOHET runs.

BC, OC, and aerosol water) are calculated in the baseline, NOHET, HETNODUST, and HETDUST simulations for the preindustrial, present-day, and year 2100 atmospheres. All aerosol forcing calculations are performed for both internal and external mixing states. We compute the direct radiative forcing of each species as the difference in the net flux with and without the species, and then calculate anthropogenic forcing in the present-day and 2100 scenarios by comparison with the preindustrial scenario. Forcing estimates at TOA and the Earth's surface are summarized in Tables 5 and 6, respectively. Note that forcing values reported here for the three time periods account for the changes in emission inventories only, since we use the same present-day climate in all the simulations.

4.1. Anthropogenic Forcing by Tropospheric O_3

[41] Annual and global mean TOA forcing by anthropogenic O_3 is estimated to be 0.22 W m^{-2} for the present-day and 0.57 W m^{-2} for year 2100 in the baseline simulations (Table 5). The global distributions of present-day and year 2100 TOA O_3 radiative forcing predicted from the baseline simulations are shown in Figure 9. Predicted geographical patterns of forcing agree with those predicted by *Mickley et al.* [1999] for the present-day atmosphere and those reported in *Gauss et al.* [2003] for year 2100. Previous global studies have generally reported O_3 radiative forcing at the tropopause to avoid the influence of stratospheric O_3. The current TOA forcings of 0.22 W m^{-2} in present-day and 0.57 W m^{-2} in year 2100 correspond to tropopause forcings of 0.50 W m^{-2} and 1.27 W m^{-2}, respectively. The present-day tropopause forcing of 0.50 W m^{-2} from the baseline simulation is close to the 0.44 W m^{-2} reported by *Mickley et al.* [1999]. The change in annual mean tropopause O_3 forcing from year 2000 to 2100 is predicted to be 0.77 W m^{-2}, which is within the range of 0.40 to 0.78 W m^{-2} obtained from 11 different models in the study of *Gauss et al.* [2003].

[42] To evaluate the effects of chemistry-aerosol coupling on estimated anthropogenic O_3 forcing, Figure 9 also shows the absolute and the percentage differences in the anthropogenic TOA O_3 forcings between the baseline and the NOHET simulations. Compared with the forcing estimates from the NOHET simulations, the annual and global mean TOA O_3 forcing from the baseline simulation is 8% lower in present-day and 16% lower in year 2100 (Table 5). Anthropogenic O_3 forcing is influenced by hydrolysis of N_2O_5 and absorption of NO_2, NO_3, and HO_2, which are significant in present-day and year 2100 but are not predicted to be important preindustrially. These heterogeneous reactions are predicted to reduce TOA anthropogenic O_3 forcing by 20–45% in present-day and by 20–32% in year 2100 at mid to high latitudes in the NH (Figure 9), corresponding to the reduction of O_3 concentrations there (see section 3.1). Mineral dust uptake has a negligible influence on estimates of anthropogenic ozone forcing. With dust concentrations assumed to be the same for all the time periods, the dust uptake reduces approximately the same amount of O_3 in all

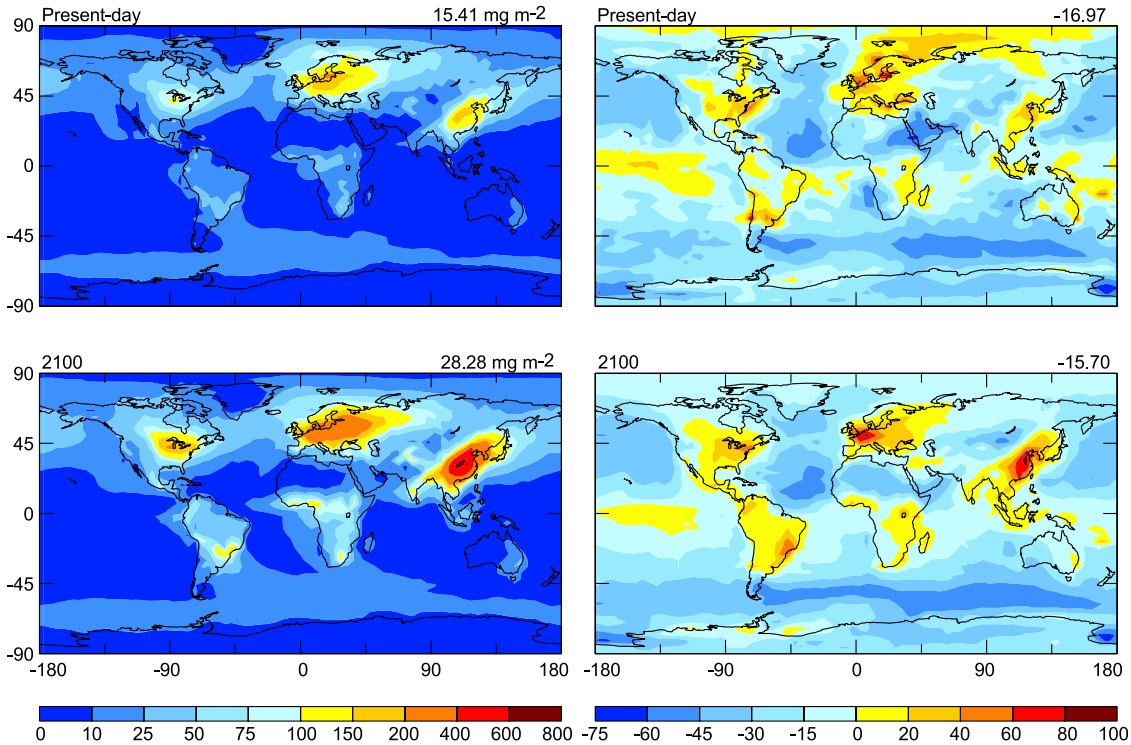

Figure 8. Predicted annual average column burdens (mg m^{-2}) of aerosol water associated with sulfate, nitrate, and OC aerosols for present-day (top left panel) and year 2100 (bottom left panel) baseline simulations. Right column shows the percentage changes in aerosol water column burdens between the baseline and the NOHET simulations in present-day (top right panel) and 2100 (bottom right panel) scenarios. All the heterogeneous reactions listed in Table 1 are considered in the baseline simulations, whereas all these heterogeneous reactions are removed in the NOHET runs.

time periods; the difference in global burden of tropospheric O_3 between the HETDUST and the NOHET simulations is 11.3, 12.8, and 13.7 Tg in the preindustrial, present-day, and year 2100 atmospheres, respectively.

[43] At the Earth's surface, O_3 shortwave forcing is globally negative, which offsets positive O_3 longwave forcing and leads to a relatively small net forcing at the surface (Table 6). The global and annual mean anthropogenic O_3 forcing at the surface is predicted to be 0.07 W m^{-2} in the present-day and 0.11 W m^{-2} in year 2100 in the baseline simulation, which increases to 0.08 W m^{-2} in present-day and 0.15 W m^{-2} in year 2100 in the absence of heterogeneous reactions.

4.2. Anthropogenic Aerosol Forcing

[44] Predicted global and annual mean TOA direct radiative forcings by individual and collective aerosols are given in Table 5. The baseline present-day anthropogenic forcing of sulfate at TOA is predicted to be -0.57 W m^{-2}. In year 2100, the predicted sulfate TOA forcing of -0.54 W m^{-2} is slightly lower than the present-day value as a result of the predicted decreases in sulfate emissions associated with IPCC SRES A2. Present-day TOA BC and OC forcings are +0.53 and -0.23 W m^{-2}, which agree closely with the +0.51 and -0.18 W m^{-2} predicted by *Chung and Seinfeld* [2002], respectively. Carbonaceous aerosols are predicted to be important in influencing year 2100 climate; while TOA OC forcing of -0.52 W m^{-2} is comparable to that by sulfate, BC is predicted to exert a strong TOA warming of 1.26 W m^{-2}. Similarly high forcings by carbonaceous aerosols in year 2100 were also reported by *Koch* [2001], who predicted a global and annual mean TOA OC forcing of -0.64 W m^{-2} and a BC forcing of 0.89–1.24 W m^{-2}, depending on the wet deposition assumptions used for BC. Present-day baseline nitrate anthropogenic forcing at TOA is predicted to be relatively small, -0.16 W m^{-2}, increasing to -0.95 Wm^{-2} in year 2100. The year 2100 nitrate forcing predicted here is lower than that of -1.28 W m^{-2} predicted by *Adams et al.* [2001]. The difference in predicted nitrate forcing between the two studies can be explained as follows. *Adams et al.* [2001] used off-line gas-phase HNO_3 fields from the Harvard-GISS GCM [*Mickley et al.*, 1999] to simulate the gas-particle partitioning of HNO_3. Although the gas-phase chemistry used in this work is basically the same as that used in the study of *Mickley et al.* [1999], the new treatments of ice scavenging of HNO_3 [*Liao et al.*, 2003] and mineral dust uptake of HNO_3 [*Liao et al.*, 2004] in this work lead to reduced gas-phase HNO_3 concentrations. Accounting for heterogeneous reactions on surface areas of sulfate, nitrate, OC, sea salt, and mineral dust leads to higher HNO_3 production from the reaction of N_2O_5 than from the hydrolysis on sulfate aerosol alone. Furthermore, the reaction of HNO_3 with sea salt aerosol increases nitrate formation along coastal zones [*Liao et al.*, 2004]. In year 2100, the predicted baseline global nitrate burden of 1.97 Tg is 10% higher than that of 1.79 Tg predicted by *Adams et al.* [2001], but the predicted TOA anthropogenic forcing in the current study is

Table 5. Summary of Ozone and Aerosol Forcings at TOA for the Baseline and Sensitivity Simulations for the Years 1800, 2000, and 2100[a]

	Direct Forcing, W m^{-2}			Anthropogenic Forcing, W m^{-2}	
Species	Preindustrial 1800	Modern Day 2000	IPCC SRES A2 2100	Modern Day 2000	IPCC SRES A2 2100
			Baseline		
O_3	0.38	0.60	0.95	0.22	0.57
	0.15(S)+0.23(L)	0.24(S)+0.36(L)	0.38(S)+0.57(L)		
SO_4^{2-}	−0.20	−0.77	−0.74	−0.57	−0.54
NO_3^-	−0.06	−0.22	−1.01	−0.16	−0.95
BC	0.03	0.56	1.29	0.53	1.26
OC	−0.03	−0.26	−0.55	−0.23	−0.52
INT	−0.26	−0.25	0.08	0.01	0.34
EXT	−0.26	−0.65	−0.87	−0.39	−0.61
			NOHET		
O_3	0.41	0.65	1.09	0.24	0.68
	0.16(S)+0.25(L)	0.26(S)+0.39(L)	0.43(S)+0.66(L)		
SO_4^{2-}	−0.33	−1.07	−1.01	−0.74	−0.68
NO_3^-	−0.11	−0.23	−1.09	−0.12	−0.98
INT	−0.43	−0.55	−0.23	−0.12	0.20
EXT	−0.44	−0.97	−1.22	−0.53	−0.78
			HETNODUST		
O_3	0.41	0.63	0.97	0.22	0.56
	0.16(S)+0.25(L)	0.25(S)+0.38(L)	0.38(S)+0.59(L)		
SO_4^{2-}	−0.25	−0.91	−0.84	−0.66	−0.59
NO_3^-	−0.11	−0.23	−1.14	−0.12	−1.03
INT	−0.36	−0.40	−0.11	−0.04	0.25
EXT	−0.36	−0.80	−1.07	−0.44	−0.71
			HETDUST		
O_3	0.39	0.63	1.07	0.24	0.68
	0.15(S)+0.24(L)	0.25(S)+0.38(L)	0.42(S)+0.65(L)		
SO_4^{2-}	−0.26	−0.91	−0.89	−0.65	−0.63
NO_3^-	−0.06	−0.21	−0.98	−0.15	−0.92
INT	−0.32	−0.37	−0.02	−0.05	0.30
EXT	−0.33	−0.79	−1.01	−0.46	−0.68

[a]Here INT, the internally mixed sulfate, nitrate, BC, OC, and aerosol water; EXT, same aerosols as in INT but aerosols are externally mixed; ozone forcing = shortwave forcing (S) + longwave forcing (L).

26% lower, because nitrate associated with sea salt aerosol has no significant contribution to radiative forcing as a result of the large size of sea salt particles.

[45] As expected, predicted anthropogenic forcing by mixed sulfate, nitrate, BC, OC, and aerosol water is quite sensitive to the mixing state of the aerosols. Based on the baseline simulations, the global and annual mean anthropogenic TOA radiative forcing by the internal mixture shows an essentially zero warming of 0.01 W m^{-2} in the present-day and a stronger heating of 0.34 W m^{-2} in year 2100, whereas that assuming an external mixture is predicted to be −0.39 W m^{-2} in present-day and −0.61 W m^{-2} in year 2100 (Table 5). Predicted TOA anthropogenic forcing by the external mixture differs from the sum of forcings by all aerosol species; on a global and annual mean basis, the baseline TOA anthropogenic forcing by the external mixture shows 0.04 W m^{-2} (or 9%) less cooling than the sum of the anthropogenic forcings in present-day, and 0.14 W m^{-2} (or 19%) less cooling in year 2100, indicating stronger radiative interactions between aerosols when aerosol burdens are higher in year 2100.

[46] Surface radiative forcing by a scattering aerosol is practically the same as its forcing at TOA (Table 6). Because of the strong absorption by BC and weak absorption by OC, the surface forcings of these two aerosols are different from their forcings at TOA. The anthropogenic OC cooling at the surface is about 56% higher than that at TOA in both present-day and year 2100. While BC has strong warming at TOA, it leads to strong cooling at the surface; the global and annual mean BC anthropogenic forcing at the surface is predicted to be −0.94 W m^{-2} in present-day and −2.20 W m^{-2} in year 2100. As a result of the largest contribution of BC to surface cooling, mixed aerosols (sulfate, nitrate, BC, and OC) are predicted to have an anthropogenic cooling of −1.98 to −2.42 W m^{-2} in present-day and −4.36 to −5.34 Wm^{-2} in year 2100, depending on the mixing state of the aerosols (Table 6).

[47] The predicted baseline geographical distributions of the annual mean TOA and surface anthropogenic forcing by all aerosols are shown in Figure 10 for both the internal and external mixtures. Strong TOA cooling is predicted over the industrialized regions; over Eastern Asia, North America, and Europe, negative forcings of 5–8 W m^{-2} are predicted in present-day, and of 10–18 W m^{-2} are predicted in year 2100. Strong TOA heating is found over the Sahara Desert, the Arctic, and the Himalayas, where absorption by BC is accentuated; TOA forcings in these areas are generally in the range of 2–5 W m^{-2} in present-day and 5–10 Wm^{-2} in year 2100 for the internal mixture, whereas they are in the range of 1–2 W m^{-2} in present-day and 2–5 Wm^{-2} in year 2100 if aerosols are externally mixed. Surface forcing is globally negative; the highest anthropogenic forcing values

Table 6. Summary of Ozone and Aerosol Forcings at the Surface for the Baseline and Sensitivity Simulations for the Years 1800, 2000, and 2100[a]

	Direct Forcing, W m^{-2}			Anthropogenic Forcing, W m^{-2}	
Species	Preindustrial 1800	Modern Day 2000	IPCC SRES A2 2100	Modern Day 2000	IPCC SRES A2 2100
			Baseline		
O_3	0.04	0.11	0.15	0.07	0.11
	−0.17(S)+0.21(L)	−0.29(S)+0.40(L)	−0.49(S)+0.64(L)		
SO_4^{2-}	−0.19	−0.77	−0.74	−0.58	−0.55
NO_3^-	−0.06	−0.21	−1.00	−0.15	−0.94
BC	−0.05	−0.99	−2.25	−0.94	−2.20
OC	−0.06	−0.42	−0.88	−0.36	−0.82
INT	−0.41	−2.83	−5.75	−2.42	−5.34
EXT	−0.37	−2.35	−4.73	−1.98	−4.36
			NOHET		
O_3	0.05	0.13	0.20	0.08	0.15
	−0.18(S)+0.23(L)	−0.33(S)+0.46(L)	−0.57(S)+0.77(L)		
SO_4^{2-}	−0.33	−1.07	−1.01	−0.74	−0.68
NO_3^-	−0.10	−0.23	−1.07	−0.13	−0.97
INT	−0.58	−3.12	−6.09	−2.54	−5.51
EXT	−0.54	−2.65	−5.06	−2.11	−4.52
			HETNODUST		
O_3	0.05	0.11	0.15	0.06	0.10
	−0.18(S)+0.23(L)	−0.31(S}+0.42(L)	−0.50(S)+0.65(L)		
SO_4^{2-}	−0.24	−0.90	−0.83	−0.66	−0.59
NO_3^-	−0.10	−0.23	−1.13	−0.13	−1.03
INT	−0.50	−2.96	−5.95	−2.46	−5.45
EXT	−0.46	−2.48	−4.93	−2.02	−4.47
			HETDUST		
O_3	0.04	0.13	0.19	0.09	0.15
	−0.17(S)+0.21(L)	−0.31(S)+0.44(L)	−0.56(S)+0.75(L)		
SO_4^{2-}	−0.26	−0.91	−0.89	−0.65	−0.63
NO_3^-	−0.06	−0.21	−0.96	−0.15	−0.90
INT	−0.47	−2.94	−5.88	−2.47	−5.41
EXT	−0.43	−2.47	−4.85	−2.04	−4.42

[a]Here INT, internally mixed sulfate, nitrate, BC, OC, and aerosol water; EXT, same aerosols as in INT but aerosols are externally mixed; ozone forcing = shortwave forcing (S) + longwave forcing (L).

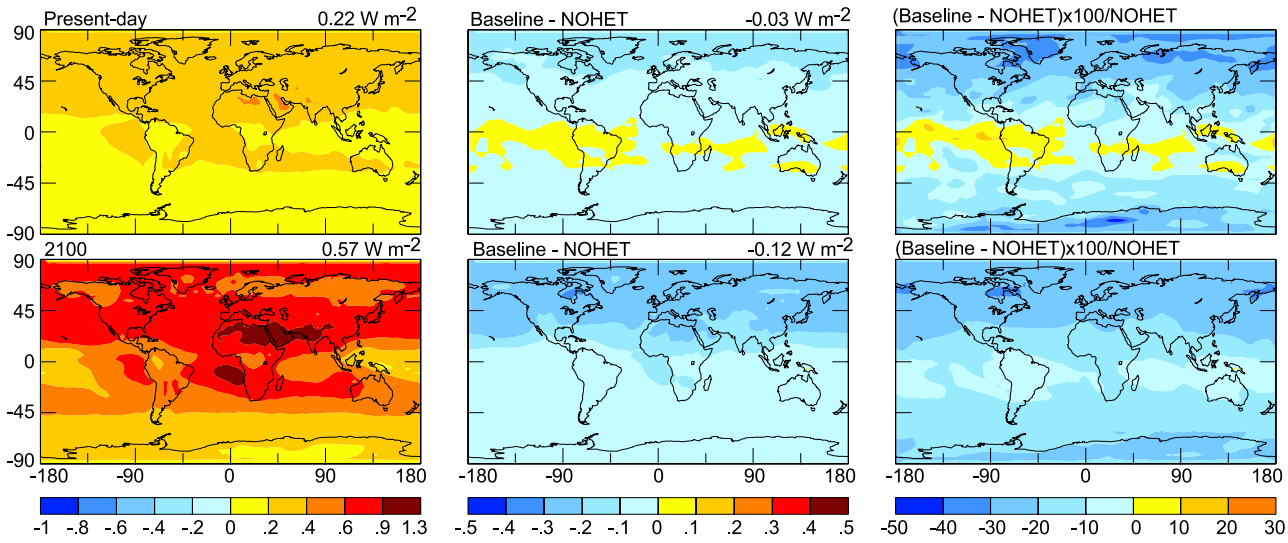

Figure 9. TOA anthropogenic radiative forcing (W m^{-2}) by tropospheric ozone obtained from the baseline simulations (left column). Middle column presents absolute differences (W m^{-2}) (Baseline-NOHET) and right column shows percentage changes ((Baseline-NOHET) × 100/NOHET) in TOA anthropogenic ozone forcings caused by heterogeneous reactions. All the heterogeneous reactions listed in Table 1 are considered in the baseline simulations, whereas all these heterogeneous reactions are removed in the NOHET runs. Upper panels are the predictions for the present-day scenario, and the bottom panels are for the year 2100 atmosphere.

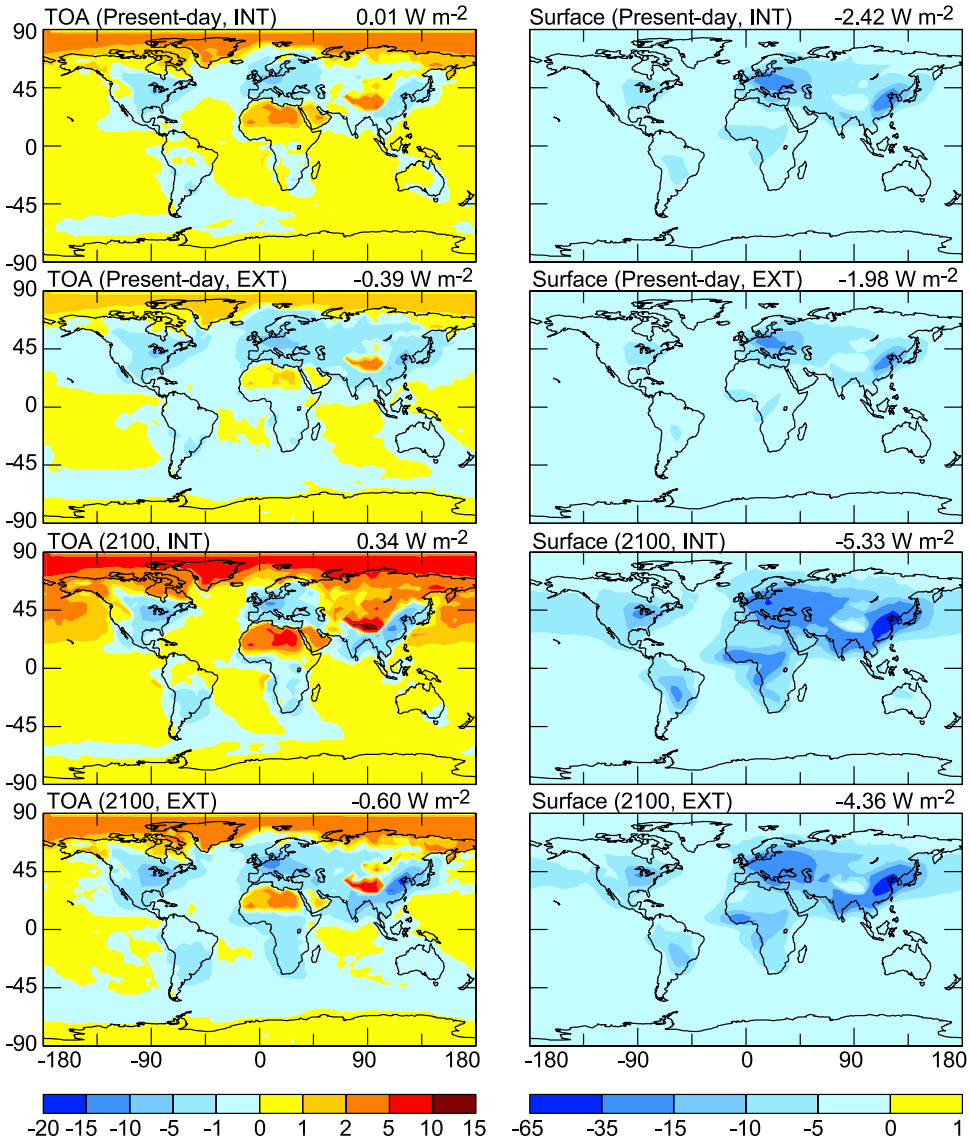

Figure 10. Predicted annual mean TOA and surface anthropogenic forcing (W m^{-2}) by mixed sulfate, nitrate, BC, OC, and aerosol water in present-day and year 2100. Predictions are based on the baseline simulations with all the heterogeneous reactions listed in Table 1. Above each panel, the time period, aerosol mixing state, and the global mean forcing value are indicated.

of −15 to −25 W m^{-2} are predicted over Eastern China and Europe in present-day, and the anthropogenic cooling is predicted to reach about 60 W m^{-2} over Eastern China in year 2100.

[48] To examine the effects of nondust and dust-associated heterogeneous reactions on anthropogenic aerosol forcing, we show in Figure 11 the differences between the TOA anthropogenic forcings by the internal mixture calculated in the baseline, HETNODUST, HETDUST simulations and those from the NOHET simulation for both the present-day and year 2100 atmospheres. Compared with the NOHET simulations, both the nondust and the dust-associated reactions increase the present-day global mean TOA aerosol forcing by 0.07 W m^{-2}, while in year 2100 the nondust heterogeneous reactions increase the global mean anthropogenic TOA aerosol forcing by 0.04 W m^{-2} and mineral dust uptake increases the TOA forcing by 0.09 W m^{-2}; hence heterogeneous reactions lead to less cooling (or more heating) by aerosols. Hydrolysis of N_2O_5 is predicted to be important in influencing anthropogenic aerosol forcing over industrialized areas. As shown in section 3.3, column burdens of nitrate aerosol over Europe, United States, and Eastern China are increased by the nondust heterogeneous reactions by 30–50% in present-day and by 10–70% in year 2100. These changes in nitrate burdens, together with the associated 20–92% changes in aerosol water in these areas (section 3.5), lead to 0–2 W m^{-2} more aerosol cooling at TOA over Europe, Eastern Asia, and United States in the present-day atmosphere than the forcings calculated in the NOHET simulation (middle panels of Figure 11). In year 2100, the hydrolysis of N_2O_5 is predicted to have a significant effect because of high aerosol concentrations and high NO_x emissions, which increases the TOA anthropogenic aerosol

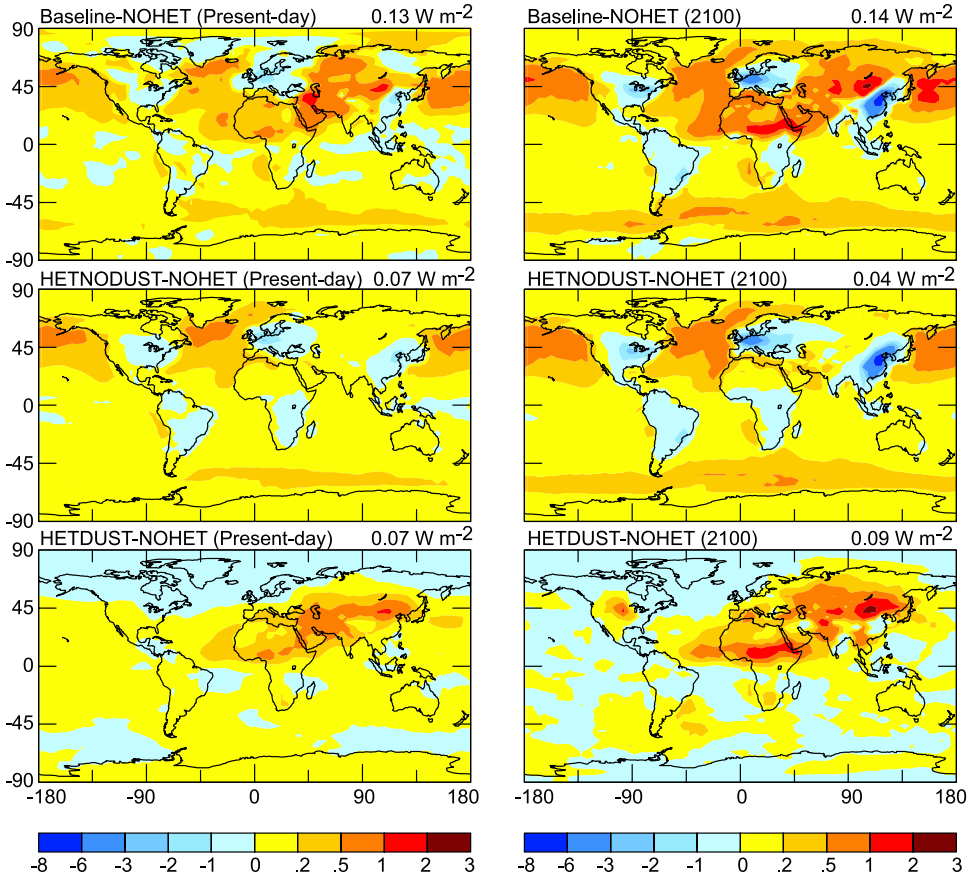

Figure 11. Differences in predicted TOA anthropogenic forcings (W m^{-2}). (a) Combined effects of both nondust and dust-associated heterogeneous reactions (baseline-NOHET), (b) effects of nondust heterogeneous reactions (HETNODUST-NOHET), and (c) effects of dust-associated heterogeneous reactions (HETDUST-NOHET). Left column is for the present-day atmosphere and the right column is for year 2100 scenario. Above each panel, the global mean value is indicated.

cooling by 3–6 W m^{-2} over Europe, 6–8 W m^{-2} in Eastern Asia, and 2–3 W m^{-2} over the United States when the forcings from the HETNODUST simulation are compared with those calculated in the NOHET simulation. The nondust reactions also lead to 0–1 W m^{-2} more TOA cooling over biomass burning regions in South America and Africa in both the present-day and year 2100.

[49] Sea salt uptake of SO_2 leads to less cooling over the oceans. In both the present-day and year 2100 scenarios, reductions of 0.5–1 W m^{-2} in TOA anthropogenic aerosol cooling occur over the oceans around 60°N (middle panels of Figure 11), where SO_2 transported from the industrialized areas is taken up by sea salt near the coastal zones and sulfate concentrations in the downwind regions are reduced. Sea salt in the SH has practically no influence on anthropogenic aerosol forcing.

[50] Because mineral dust uptake reduces sulfate and nitrate concentrations and associated aerosol water near the Sahara, central, and northeast Asia, anthropogenic aerosol forcings in and near these areas generally exhibit less TOA cooling (or stronger heating) of about 0.5–1 W m^{-2} in the present-day and of about 1–2 W m^{-2} in year 2100 (bottom panels of Figure 11). When the effects of both the nondust and dust-associated heterogeneous reactions are combined (top panels of Figure 11), although the nondust and dust-associated reactions can interact, the interactions do not have a large impact on the quantitative results obtained when these two types of reactions are considered separately.

[51] Although TOA anthropogenic forcings calculated for the external mixture are quite different from those calculated for the internal mixture, the effects of heterogeneous reactions on TOA anthropogenic forcing by the external mixture (not shown) are similar to those shown in Figure 11 for the internal mixture. Locations and magnitudes of changes in TOA anthropogenic aerosol forcings are practically the same for the two different mixing states. Compared with the NOHET simulations, while the nondust and dust-associated reactions increase the present-day global mean TOA forcing by 0.08 and 0.07 W m^{-2}, respectively, they increase the year 2100 global mean TOA forcing by 0.07 and 0.09 W m^{-2}, respectively (Table 5). At the surface layer, the effects of heterogeneous reactions on anthropogenic forcing are similar to those predicted for TOA forcings. Because heterogeneous reactions mainly influence burdens of sulfate and nitrate aerosols whose forcings at TOA are about the same as those at the surface, predicted changes in surface anthropogenic forcing by heterogeneous reactions are geographically and quantitatively similar to those shown in Figure 11.

Table 7. Comparisons of the Simulated Global and Annual Mean TOA Anthropogenic Aerosol Forcing With Other Studies

	Anthropogenic Forcing, W m^{-2}	
	Present-Day	2100 (IPCC SRES A2)
Sulfate		
This work	−0.57	−0.54
Koch [2001]	−0.65	−0.54
Adams et al. [2001]	−0.95	−0.85
Boucher and Anderson [1995]	−0.29	
Feichter et al. [1997]	−0.35	
Penner et al. [1998]	−0.81	
Kiehl et al. [2000]	−0.56	
Jacobson [2001]	−0.31	
Takemura et al. [2002]	−0.20	
OC		
This work	−0.23	−0.52
Koch [2001]	−0.30	−0.64
Jacobson [2001]	−0.06	
Chung and Seinfeld [2002]	−0.18	
Takemura et al. [2002]	−0.26	
BC		
This work	0.53	1.26
Haywood and Ramaswamy [1998]	0.40	
Koch [2001]	0.35	0.89–1.24
Jacobson [2001]	0.52	
Chung and Seinfeld [2002]	0.51	
Takemura et al. [2002]	0.42	
Nitrate		
This work	−0.16	−0.95
Adams et al. [2001]	−0.19	−1.28
Jacobson [2001]	−0.04	
EXT[a]		
This work	−0.39	−0.61
Hansen et al. [2005]	−0.44	

[a]Externally mixed sulfate, nitrate, BC, and OC.

4.3. Comparisons of Predicted Radiative Forcing With Other Studies

[52] Table 7 compares the predicted TOA anthropogenic forcing by individual aerosol species and by mixed aerosols with the estimates in previous studies. TOA anthropogenic forcings predicted in this work lie within the ranges of previous predictions. Differences in the estimates among studies arise mainly from differences in simulated aerosol column burdens and the prescribed extinction efficiency depending on the relative humidity and aerosol size. It should be noted that comparisons of annual and global mean forcing values are not necessarily indicative of differences in predicted seasonal variations and geographical distributions.

5. Uncertainties and Sensitivities

[53] There are numerous sources of uncertainty in the calculated burdens, heterogeneous reactions, and radiative forcing. First, the version of the GISS GCM used in this work has a relatively coarse horizontal resolution of 4° latitude by 5° longitude and nine σ layers in the vertical, from surface to 10 mbar. Since heterogeneous reactions are important where aerosol concentrations are high, a coarse resolution model could predict less significant effects of heterogeneous reactions near emission sources and stronger effects in areas away from sources than a model with fine resolution.

[54] The results presented in the previous sections indicate that heterogeneous reactions are influential in anthropogenic forcing, especially in the year 2100 atmosphere. Because the year 2100 simulations are based on the IPCC SRES A2, the scenario with the most significant projected increases in emissions, the effects of heterogeneous reactions on radiative forcings presented in this work for year 2100 should be taken to represent upper limit estimates.

[55] Uncertainties in model results also arise from the fixed present-day climate used for predicting the preindustrial and year 2100 concentrations and forcings of ozone and aerosols. The changes in concentrations of greenhouse gases, ozone, and aerosols from the preindustrial time to year 2100 should influence both climate and abundances of ozone and aerosols, which are expected to have impacts on estimated forcings. While in this work we study the preindustrial, present-day, and year 2100 forcings only by using different emission scenarios, further simulations show that burdens of ozone and aerosols are reduced in a warmer climate with increased temperature and precipitation if emissions are kept at the present-day levels. Such interactions among gas-phase chemistry, aerosols, and climate will be reported subsequently.

[56] The forcing estimates presented in this work are based on assumed size distributions, refractive indices, and mixing states of aerosols. By assuming that aerosols are either internally or externally mixed, we have shown that aerosol radiative forcings are very sensitive to mixing state. The actual mixing state of aerosols in the atmosphere is a complicated phenomenon that depends on the aging and coagulation of aerosol particles, and internal and external mixtures can coexist in the atmosphere. In our work the refractive index of the internal mixture is calculated by volume weighting as in most previous studies, but such linear combination is an oversimplified assumption.

[57] For heterogeneous reactions, the results presented in this work rely on uptake coefficients, some of which have large uncertainties. For example, although we follow the study of *Evans and Jacob* [2005] to calculate $\gamma(N_2O_5)$ as a function of aerosol type, relative humidity, and temperature, the humidity and temperature dependence of $\gamma(N_2O_5)$ on sulfate aerosol is based on the measurements for ammonium sulfate [*Evans and Jacob*, 2005]. The relationship between the heterogeneous uptake of N_2O_5 and relative humidity has been shown to be different for ammonium sulfate, ammonium bisulfate, and sulfuric acid aerosols [*Kane et al.*, 2001]. Furthermore, we assume that nitrate has the same $\gamma(N_2O_5)$ as ammonium sulfate in this work, but *Hallquist et al.* [2003] reported that $\gamma(N_2O_5)$ values could be lower by an order of magnitude compared to those for uptake on the sulfate aerosols. To see the impacts of these assumptions on model results, we performed a sensitivity simulation with $\gamma(N_2O_5)$ values on sulfate/ammonium/nitrate aerosols in the year 2100 baseline simulation reduced to 10% of the values obtained from equation (1). This simulation shows that the effects of N_2O_5 reaction on O_3 at high latitudes and on nitrate formation are not sensitive to $\gamma(N_2O_5)$. Compared with the year 2100 NOHET simulation, while the annual mean total ozone mass over 45–90°N is reduced by 26.1% in the baseline simulation, it is reduced by 23.0% in this sensitivity study. The column burdens of nitrate aerosol over Europe and Eastern China with the reduced $\gamma(N_2O_5)$ on sulfate/nitrate/ammonium differ from those from the base-

line simulation by less than 10%. *Dentener and Crutzen* [1993] and *Schaap et al.* [2004] also reported that the N_2O_5 reaction is not sensitive to $\gamma(N_2O_5)$.

[58] The laboratory-determined uptake coefficients for the heterogeneous reactions on mineral dust have larger uncertainties than those on nondust aerosols. For example, *Underwood et al.* [2001] proposed a $\gamma(HNO_3)$ of $2.5 \pm 0.1 \times 10^{-4}$ on dry dust and found that $\gamma(HNO_3)$ increases with relative humidity, whereas *Hanisch and Crowley* [2001] recommended a $\gamma(HNO_3)$ of 0.1. *Bauer et al.* [2004] have investigated the sensitivity of global ozone burden to heterogeneous reactions of HNO_3, NO_3, N_2O_5, and O_3 on mineral dust and concluded that the reaction of HNO_3 plays the most important role in influencing global ozone, however they found that the global ozone burden does not change when $\gamma(HNO_3)$ is varied between 0.05 and 0.25. We performed additional sensitivity studies to examine the sensitivity of nondust sulfate and nitrate formation to $\gamma(HNO_3)$ and $\gamma(SO_2)$ on mineral dust. With $\gamma(SO_2)$ values on mineral dust reduced to 10% of the values shown in Table 1, year 2100 sulfate column burdens near the Sahara Desert still show 80–90% of the reductions predicted in the baseline simulation. In another sensitivity study with $\gamma(HNO_3)$ reduced from 0.1 in the baseline simulation to 0.01, the reductions in year 2100 nitrate column burdens near the Sahara Desert are 70–80% of the reductions predicted in the baseline simulation. Thus we conclude that the effects of heterogeneous reactions on mineral dust presented in this study are still important regionally if the assumed uptake coefficients on dust are reduced by an order of magnitude.

[59] The uptake coefficient for the uptake of SO_2 on sea salt also has large uncertainties. While we use $\gamma(SO_2)$ of 0.05 for RH > 50% and 0.005 when RH < 50% following the study of *Song and Carmichael* [2001], *Chameides* [1984] and *van den Berg et al.* [2000] used 0.11. As discussed in *Liao et al.* [2004], the sea salt uptake of SO_2 calculated in our model may represent an upper limit because we assume pH of 7.0 for sea salt particles. We tested here how the predicted sulfate reductions over the oceans depend on the choice of $\gamma(SO_2)$ on sea salt. When $\gamma(SO_2)$ values on sea salt are reduced to 10% of those given in Table 1, the predicted reductions in year 2100 sulfate column burdens over oceans are 60–70% of those predicted in the baseline simulation.

[60] Finally, it should also be mentioned that we did not account for all the heterogeneous reactions in the atmosphere. For example, soot aerosol could take up HNO_3 and ammonium bisulfate could take up PAN [*Jacob*, 2000]. These reactions should be considered when more laboratory studies are available.

6. Summary and Conclusions

[61] The GISS GCM II' with fully coupled tropospheric chemistry and aerosols has been used to simulate the concentrations of O_3 and aerosols in preindustrial time, present-day, and year 2100 based on the IPCC SRES A2. The model includes: (1) a detailed simulation of tropospheric O_3-NO_x-hydrocarbon chemistry; (2) the prediction of sulfate/nitrate/ammonium/sea salt/water, black carbon, primary organic carbon, secondary organic carbon, and mineral dust aerosols; (3) heterogeneous reactions of N_2O_5, NO_3, NO_2, and HO_2 on wet aerosols; (4) uptake of SO_2 by sea salt; (5) uptake of SO_2, HNO_3 and O_3 by mineral dust; and (6) effects of aerosols on gas-phase photolysis rates. The model has been used to estimate anthropogenic radiative forcing by O_3 and aerosols and to examine the effects of heterogeneous reactions on these forcings.

[62] Considering heterogeneous reactions, anthropogenic O_3 is predicted to have a globally and annually averaged present-day TOA forcing of +0.22 W m^{-2} and year 2100 forcing of +0.57 W m^{-2}. Net anthropogenic TOA forcing by internally mixed sulfate, nitrate, OC, and BC aerosols is estimated to be virtually zero in the present-day and +0.34 W m^{-2} in year 2100, whereas it is predicted to be −0.39 W m^{-2} in present-day and −0.61 W m^{-2} in year 2100 if the aerosols are externally mixed. Surface forcing from all aerosols together is predicted to be −1.98 to −2.42 W m^{-2} in present-day and −4.36 to −5.34 W m^{-2} in year 2100, depending on the mixing state.

[63] Hydrolysis of N_2O_5 and aerosol absorption of NO_2, NO_3, and HO_2 are significant factors in present-day and year 2100 but are not important in the preindustrial atmosphere. Compared to forcings calculated in the absence of heterogeneous reactions, the nondust reactions generally lead to a reduction in the predicted TOA anthropogenic O_3 forcing by 20–45% in present-day and by 20–32% in year 2100 at mid to high latitudes in the Northern Hemisphere. Although mineral dust uptake of HNO_3 and O_3 leads to a reduction of O_3 concentrations near dust sources by 10–15%, dust uptake has practically no influence on estimates of global anthropogenic O_3 forcing, because the change in ozone mass by the dust-associated heterogeneous reactions is about the same in all the three periods.

[64] Reactions of N_2O_5, NO_3, NO_2, and HO_2 on aerosols are found to be important in estimating the anthropogenic forcing over the industrialized areas, especially in the IPCC SRES A2 scenario for 2100; ignoring them leads to an underestimate of anthropogenic aerosol cooling by 3–6 W m^{-2} over Europe, 6–8 W m^{-2} in Eastern Asia, and 2–3 W m^{-2} over the United States.

[65] Sea salt uptake of SO_2 leads to less cooling of 0.5–1 W m^{-2} over the oceans around 60°N in the present-day and year 2100 scenarios. Sea salt uptake is not important in the Southern Hemisphere where concentrations of anthropogenic sulfate are low. Mineral dust aerosol reduces sulfate and nitrate concentrations and associated aerosol water near the Sahara, central and northeast Asia, producing less anthropogenic aerosol cooling (or stronger heating) of 0.5–1 W m^{-2} in the present-day and of 1–2 W m^{-2} in year 2100 near dust sources.

[66] Results presented in this work suggest that heterogeneous reactions have important impacts on regional concentrations and forcings of ozone and aerosols. Among the reactions investigated in this work, hydrolysis of N_2O_5 is shown to be the most important process that influences ozone and nitrate formation. Although this reaction has been included in most current global models, it is generally considered to take place on sulfate aerosol only. Hydrolysis of N_2O_5 on other aerosols, as well as the dependence of $\gamma(N_2O_5)$ on temperature and relative humidity should also be considered. Inclusion of mineral dust uptake of O_3, SO_2, and HNO_3 and sea salt uptake of SO_2 appears to be called

for, subject to refinements as new laboratory measurements become available.

[67] **Acknowledgments.** This work was supported by the NASA Earth Observing System – Interdisciplinary Science Program (NASAEOS-IDS). We would also like to acknowledge the Center for Advanced Computing Research at Caltech for computing resources.

References

Adams, P. J., J. H. Seinfeld, D. M. Koch, L. Mickley, and D. Jacob (2001), General circulation model assessment of direct radiative forcing by the sulfate-nitrate-ammonium-water inorganic aerosol system, *J. Geophys. Res.*, *106*, 1097–1111.

Andreae, M. O., and P. J. Crutzen (1997), Atmospheric aerosols: Biogeochemical sources and role in atmospheric chemistry, *Science*, *276*, 1052–1058.

Atkinson, R., D. L. Baulch, R. A. Cox, J. N. Crowley, R. F. Hampson Jr., M. E. Jenkin, J. A. Kerr, M. J. Rossi, and J. Troe (2004), Summary of evaluated kinetic and photochemical data for atmospheric chemistry, Cambridge Univ., Cambridge, UK. (Available at http://www.iupac-kinetic.ch.cam.ac.uk/summary/IUPACsumm_web_latest.pdf)

Bauer, S. E., Y. Balkanski, M. Schulz, D. A. Hauglustaine, and F. Dentener (2004), Global modeling of heterogeneous chemistry on mineral aerosol surfaces: Influence on tropospheric ozone chemistry and comparison to observations, *J. Geophys. Res.*, *109*, D02304, doi:10.1029/2003JD003868.

Benkovitz, C. M., M. T. Scholtz, J. Pacyna, L. Tarrason, J. Dignon, E. C. Voldner, P. A. Spiro, J. A. Logan, and T. E. Graedel (1996), Global gridded inventories of anthropogenic emissions of sulfur and nitrogen, *J. Geophys. Res.*, *101*, 29,239–29,253.

Bian, H. S., and C. S. Zender (2003), Mineral dust and global tropospheric chemistry: Relative roles of photolysis and heterogeneous uptake, *J. Geophys. Res.*, *108*(D21), 4672, doi:10.1029/2002JD003143.

Boucher, O., and T. L. Anderson (1995), General circulation model assessment of the sensitivity of direct climate forcing by anthropogenic sulfate aerosols to aerosol size and chemistry, *J. Geophys. Res.*, *100*, 26,117–26,134.

Bouwman, A. F., D. S. Lee, W. A. H. Asman, F. J. Dentener, K. W. VanderHoek, and J. G. J. Olivier (1997), A global high-resolution emission inventory for ammonia, *Global Biogeochem. Cycles*, *11*, 561–587.

Castro, T., L. G. Ruizsuarez, J. C. Ruizsuarez, M. J. Molina, and M. Montero (1997), Sensitivity analysis of a UV-radiation transfer model and experimental photolysis rates of NO_2 in the atmosphere of Mexico City, *Atmos. Environ.*, *31*, 609–620.

Chameides, W. L. (1984), Photochemistry of a remote marine stratiform cloud, *J. Geophys. Res.*, *89*, 4739–4755.

Chin, M., P. Ginoux, S. Kinne, O. Torres, B. Holben, B. Duncan, R. Martin, J. Logan, A. Hiragushi, and T. Nakajima (2002), Tropospheric aerosol optical thickness from the GOCART model and comparisons with satellite and sunphotometer measurements, *J. Atmos. Sci.*, *59*, 461–483.

Chung, S. H., and J. H. Seinfeld (2002), Global distribution and climate forcing of carbonaceous aerosols, *J. Geophys. Res.*, *107*(D19), 4407, doi:10.1029/2001JD001397.

Collins, W. D., P. J. Rasch, B. E. Eaton, B. V. Khattatov, J.-F. Lamarque, and C. S. Zender (2001), Simulating aerosols using a chemical transport model with assimilation of satellite aerosol retrievals: Methodology for INDOEX, *J. Geophys. Res.*, *106*, 7313–7336.

Cooke, W. F., C. Liousse, H. Cachier, and J. Feichter (1999), Construction of a $1° \times 1°$ fossil fuel emission data set for carbonaceous aerosol and implementation and radiative impact in the ECHAM4 model, *J. Geophys. Res.*, *104*, 22,137–22,162.

Del Genio, A. D., and M.-S. Yao (1993), Efficient cumulus parameterization for long-term climate studies: The GISS scheme, in *The Representation of Cumulus Convection in Numerical Models*, *Meteorol. Monogr.*, vol. 46, edited by K. A. Emanuel and D. J. Raymond, pp. 181–184, Am. Meteorol. Soc., Boston, Mass.

Del Genio, A. D., M.-S. Yao, W. Kovari, and K. K.-W. Lo (1996), A prognostic cloud water parameterization for global climate models, *J. Clim.*, *9*, 270–304.

Demerjian, K. L., K. L. Schere, and J. T. Peterson (1980), Theoretical estimates of actinic (spherially integrated) flux and photolytic rate constants of atmospheric species in the lower troposphere, *Adv. Environ. Sci. Technol.*, *10*, 369–459.

Dentener, F. J., and P. J. Crutzen (1993), Reaction of N_2O_5 on tropospheric aerosols: Impact on the global distributions of NO_x, O_3, and OH, *J. Geophys. Res.*, *98*, 7149–7163.

Dentener, F. J., G. R. Carmichael, Y. Zhang, J. Lelieveld, and P. J. Crutzen (1996), Role of mineral aerosol as a reactive surface in the global troposphere, *J. Geophys. Res.*, *101*, 22,869–22,889.

Derwent, R. G., W. J. Collins, M. E. Jenkin, C. E. Johnson, and D. S. Stevenson (2003), The global distribution of secondary particulate matter in a 3-D Lagrangian chemistry transport model, *J. Atmos. Chem.*, *44*, 57–95.

Dickerson, R. R., S. Kondragunta, G. Stenchikov, K. L. Civerolo, B. G. Doddridge, and B. N. Holben (1997), The impact of aerosols on solar ultraviolet-radiation and photochemical smog, *Science*, *215*, 827–830.

Evans, M. J., and D. J. Jacob (2005), Impact of new laboratory studies of N_2O_5 hydrolysis on global model budgets of tropospheric nitrogen oxides, ozone, and OH, *Geophys. Res. Lett.*, *32*, L09813, doi:10.1029/2005GL022469.

Feichter, J., U. Lohmann, and I. Schult (1997), The atmospheric sulfur cycle in ECHAM-4 and its impact on the shortwave radiation, *Clim. Dyn.*, *13*, 235–246.

Fenter, F. F., F. Caloz, and M. J. Rossi (1995), Experimental evidence for efficient dry deposition of nitric acid on calcite, *Atmos. Environ.*, *29*, 3365–3372.

Fiore, A. M., D. J. Jacob, H. Liu, R. M. Yantosca, T. D. Fairlie, and Q. Li (2003), Variability in surface ozone background over the United States: Implications for air quality policy, *J. Geophys. Res.*, *108*(D24), 4787, doi:10.1029/2003JD003855.

Galy-Lacaux, C., and A. I. Modi (1998), Precipitation chemistry in the Sahelian savanna of Niger, Africa, *J. Atmos. Chem.*, *30*, 319–343.

Galy-Lacaux, C., G. R. Carmichael, C. H. Song, J. P. Lacaux, H. Al Ourabi, and A. I. Modi (2001), Heterogeneous processes involving nitrogenous compounds and Saharan dust inferred from measurements and model calculations, *J. Geophys. Res.*, *106*, 12,559–12,578.

Gauss, M., et al. (2003), Radiative forcing in the 21st century due to ozone changes in the troposphere and the lower stratosphere, *J. Geophys. Res.*, *108*(D9), 4292, doi:10.1029/2002JD002624.

Ghan, S., N. Laulainen, R. Easter, R. Wagener, S. Nemesure, E. Chapman, Y. Zhang, and R. Leung (2001), Evaluation of aerosol direct radiative forcing in MIRAG, *J. Geophys. Res.*, *106*, 5295–5316.

Gong, S. L., L. A. Barrie, J. M. Prospero, D. L. Savoie, G. P. Ayers, J. P. Blanchet, and L. Spacek (1997), Modeling sea-salt aerosols in the atmosphere: 2. Atmospheric concentrations and fluxes, *J. Geophys. Res.*, *102*, 3819–3830.

Goodman, A. L., G. M. Underwood, and V. H. Grassian (2000), A laboratory study of the heterogeneous reaction of nitric acid on calcium carbonate particles, *J. Geophys. Res.*, *105*, 29,053–29,064.

Goodman, A. L., E. T. Bernard, and V. H. Grassian (2001), Spectroscopic study of nitric acid and water adsorption on oxide particles: Enhanced nitric acid uptake kinetics in the presence of adsorbed water, *J. Phys. Chem. A*, *105*(26), 6443–6457.

Griffin, R. J., D. R. Cocker, J. H. Seinfeld, and D. Dabdub (1999a), Estimate of global atmospheric organic aerosol from oxidation of biogenic hydrocarbons, *Geophys. Res. Lett.*, *26*, 2721–2724.

Griffin, R. J., D. R. Cocker, R. C. Flagan, and J. H. Seinfeld (1999b), Organic aerosol formation from the oxidation of biogenic hydrocarbons, *J. Geophys. Res.*, *104*, 3555–3567.

Grini, A., G. Myhre, J. K. Sundet, and I. S. A. Isaksen (2002), Modeling the annual cycle of sea salt in the global 3D model Oslo CTM2: Concentrations, fluxes, and radiative impact, *J. Clim.*, *15*, 1717–1730.

Hallquist, M., D. J. Stewart, S. K. Stephenson, and R. A. Cox (2003), Hydrolysis of N_2O_5 on sub-micron sulfate aerosols, *Phys. Chem. Chem. Phys.*, *5*(16), 3453–3463.

Hanisch, F., and J. N. Crowley (2001), Heterogeneous reactivity of gaseous nitric acid on Al_2O_3, $CaCO_3$, and atmospheric dust samples: A Knudsen cell study, *J. Phys. Chem. A*, *105*, 3096–3106.

Hanisch, F., and J. N. Crowley (2003), Heterogeneous reactivity of NO and HNO_3 on mineral dust in the presence of ozone, *Phys. Chem. Chem. Phys.*, *5*(5), 883–887.

Hansen, J., G. Russell, D. Rind, P. Stone, A. Lacis, S. Lebedeff, R. Ruedy, and L. Travis (1983), Efficient three-dimensional global models for climate studies: Models I and II, *Mon. Weather Rev.*, *111*, 609–662.

Hansen, J., et al. (2005), Efficacy of climate forcings, *J. Geophys. Res.*, doi:10.1029/2005JD005776, in press.

Haywood, J. M., and V. Ramaswamy (1998), Global activity studies of the direct forcing due to anthropogenic sulfate and black carbon aerosols, *J. Geophys. Res.*, *103*, 6043–6058.

Intergovernmental Panel on Climate Change (IPCC) (2001), *Climate Change 2001*, edited by J. T. Houghton et al., Cambridge Univ. Press, New York.

Jacob, D. J. (2000), Heterogeneous chemistry and tropospheric ozone, *Atmos. Environ.*, 2131–2159.

Jacobson, M. Z. (1998), Studying the effects of aerosols on vertical photolysis rate coefficient and temperature profiles over an urban airshed, *J. Geophys. Res.*, *103*, 10,593–10,604.

Jacobson, M. Z. (2001), Global direct radiative forcing due to multicomponent anthropogenic and natural aerosols, *J. Geophys. Res.*, *106*, 1551–1568.

Kane, S. M., F. Caloz, and M. T. Leu (2001), Heterogeneous uptake of gaseous N_2O_5 by $(NH_4)_2SO_4$, NH_4HSO_4, and H_2SO_4 aerosol, *J. Phys. Chem. A.*, *105*(26), 6465–6470.

Kiehl, J. T., T. L. Schneider, P. J. Rasch, M. C. Barth, and J. Wong (2000), Radiative forcing due to sulfate aerosols from simulations with the National Center for Atmospheric Research Community Climate Model, Version 3, *J. Geophys. Res.*, *105*, 1441–1457.

Koch, D. M. (2001), Transport and direct radiative forcing of carbonaceous and sulfate aerosols in the GISS GCM, *J. Geophys. Res.*, *106*, 20,311–20,332.

Koch, D. M., D. Jacob, I. Tegen, D. Rind, and M. Chin (1999), Tropospheric sulfur simulation and sulfate direct radiative forcing in the Goddard Institute for Space Studies general circulation model, *J. Geophys. Res.*, *104*, 23,799–23,822.

Lacis, A. A., and J. E. Hansen (1974), A parameterization for the absorption of solar radiation in the earth's atmosphere, *J. Aerosol Sci.*, *31*, 118–133.

Lacis, A. A., and M. I. Mishchenko (1995), Climate forcing, climate sensitivity, and climate response: A radiative modeling perspective on atmospheric aerosols, in *Aerosol Forcing of Climate*, edited by R. J. Charlson and J. Heintzenberg, pp. 11–42, John Wiley, Hoboken, N. J.

Lacis, A. A., and V. Oinas (1991), A description of the correlated k-distribution method for modeling nongray gaseous absorption, thermal emission, and multiple-scattering in vertically inhomogeneous atmospheres, *J. Geophys. Res.*, *96*, 9027–9063.

Landgraf, J., and P. J. Crutzen (1998), An efficient method for online calculations of photolysis and heating rates, *J. Atmos. Sci.*, *55*, 863–878.

Lantz, K. O., R. E. Shetter, C. A. Cantrell, S. J. Flocke, J. G. Calvert, and S. Madronich (1996), Theoretical, actinometric, and radiometric determinations of the photolysis rate coefficient of NO_2 during the Mauna Loa Observatory Photochemistry Experiment 2, *J. Geophys. Res.*, *101*, 14,613–14,629.

Lelieveld, J., and R. Van Dorland (1995), Ozone chemistry changes in the troposphere and consequent radiative forcing of climate, in *Atmospheric Ozone as a Climate Gas*, edited by W. C. Wang and I. S. A. Isaksen, pp. 227–258, Springer, New York.

Liao, H., Y. L. Yung, and J. H. Seinfeld (1999), Effects of aerosols on tropospheric photolysis rates in clear and cloudy atmospheres, *J. Geophys. Res.*, *104*, 23,697–23,707.

Liao, H., P. J. Adams, S. H. Chung, J. H. Seinfeld, L. J. Mickley, and D. J. Jacob (2003), Interactions between tropospheric chemistry and aerosols in a unified general circulation model, *J. Geophys. Res.*, *108*(D1), 4001, doi:10.1029/2001JD001260.

Liao, H., J. H. Seinfeld, P. J. Adams, and L. J. Mickley (2004), Global radiative forcing of coupled tropospheric ozone and aerosols in a unified general circulation model, *J. Geophys. Res.*, *109*, D16207, doi:10.1029/2003JD004456.

Limbeck, A., and H. Puxbaum (2000), Dependence of in-cloud scavenging of polar organic aerosol compounds on the water solubility, *J. Geophys. Res.*, *105*, 19,857–19,867.

Liousse, C., J. E. Penner, C. Chuang, J. J. Walton, H. Eddleman, and H. Cachier (1996), A global three-dimensional model study of carbonaceous aerosols, *J. Geophys. Res.*, *101*, 19,411–19,432.

Martin, R. V., D. J. Jacob, R. M. Yantosca, M. Chin, and P. Ginoux (2003), Global and regional decreases in tropospheric oxidants from photochemical effects of aerosols, *J. Geophys. Res.*, *108*(D3), 4097, doi:10.1029/2002JD002622.

Metzger, S., F. Dentener, S. Pandis, and J. Lelieveld (2002a), Gas/aerosol partitioning: 1. A computationally efficient model, *J. Geophys. Res.*, *107*(D16), 4312, doi:10.1029/2001JD001102.

Metzger, S., F. Dentener, M. Krol, A. Jeuken, and J. Lelieveld (2002b), Gas/aerosol partitioning: 2. Global modeling results, *J. Geophys. Res.*, *107*(D16), 4313, doi:10.1029/2001JD001103.

Mickley, L. J., P. Murti, D. Jacob, J. Logan, and D. Rind (1999), Radiative forcing from tropospheric ozone calculated with a unified chemistry-climate model, *J. Geophys. Res.*, *104*, 30,153–30,172.

Mickley, L. J., D. J. Jacob, B. D. Field, and D. Rind (2004), Climate response to the increase in tropospheric ozone since preindustrial times: A comparison between ozone and equivalent CO_2 forcings, *J. Geophys. Res.*, *109*, D05106, doi:10.1029/2003JD003653.

Nakicenovic, N., et al. (2000), *Special Report on Emission Scenarios, Special Report of Working Group III of the Intergovernmental Panel on Climate Change*, Cambridge Univ. Press, New York.

Nenes, A., C. Pilinis, and S. N. Pandis (1998), Isorropia: A new thermodynamic equilibrium model for multiphase multicomponent inorganic aerosols, *Aquat. Geochem.*, *4*, 123–152.

Penner, J. E., C. C. Chuang, and K. Grant (1998), Climate forcing by carbonaceous and sulfate aerosols, *Clim. Dyn.*, *14*, 839–851.

Rind, D., and J. Lerner (1996), The use of on-line tracers as a diagnostic tool in general circulation model development: 1. Horizontal and vertical transport in the troposphere, *J. Geophys. Res.*, *101*, 12,667–12,683.

Rind, D., J. Lerner, K. Shah, and R. Suozzo (1999), Use of on-line tracers as a diagnostic tool in general circulation model development: 2. Transport between the troposphere and stratosphere, *J. Geophys. Res.*, *104*, 9151–9167.

Robinson, R. A., and R. H. Stokes (1965), *Electrolyte Solutions*, 2nd ed., Butterworths, London.

Ruggaber, A., R. Dlugir, and T. Nakajima (1994), Modeling radiation quantities and photolysis frequencies in the atmosphere, *J. Atmos. Chem.*, *18*, 171–210.

Schaap, M., M. van Loon, H. M. ten Brink, F. J. Dentener, and P. J. H. Builtjes (2004), Secondary inorganic aerosol simulations for Europe with special attention to nitrate, *Atmos. Chem. Phys.*, *4*, 857–874.

Schult, I., J. Feichter, and W. F. Cooke (1997), Effect of black carbon and sulfate aerosols on the global radiation budget, *J. Geophys. Res.*, *102*, 30,107–30,117.

Song, C. H., and G. R. Carmichael (2001), A three-dimensional modeling investigation of the evolution processes of dust and sea-salt particles in east Asia, *J. Geophys. Res.*, *106*, 18,131–18,154.

Tabazadeh, A., M. Z. Jacobson, H. B. Singh, O. B. Toon, J. S. Linn, R. B. Chatfield, A. N. Thakur, R. W. Talbot, and J. E. Dibb (1998), Nitric acid scavenging by mineral and biomass burning aerosols, *Geophys. Res. Lett.*, *25*, 4185–4188.

Takemura, T., T. Nakajima, O. Dubovik, B. N. Holben, and S. Kinne (2002), Single-scattering albedo and radiative forcing of various aerosol species with a global three-dimensional model, *J. Clim.*, *15*, 333–352.

Tegen, I., and A. A. Lacis (1996), Modeling of particle size distribution and its influence on the radiative properties of mineral dust aerosol, *J. Geophys. Res.*, *101*, 19,237–19,244.

Tegen, I., D. Koch, A. A. Lacis, and M. Sato (2000), Trends in tropospheric aerosol loads and corresponding impact on direct radiative forcing between 1950 and 1990: A model study, *J. Geophys. Res.*, *105*, 26,971–26,989.

Thornton, J. A., C. F. Braban, and J. P. D. Abbatt (2003), N_2O_5 hydrolysis on sub-micron organic aerosols: The effect of relative humidity, particle phase, and particle size, *Phys. Chem. Chem. Phys.*, *5*(20), 4593–4603.

Tie, X., S. Madronich, S. Walters, D. P. Edwards, P. Ginoux, N. Mahowald, R. Y. Zhang, C. Lou, and G. Brasseur (2005), Assessment of the global impact of aerosols on tropospheric oxidants, *J. Geophys. Res.*, *110*, D03204, doi:10.1029/2004JD005359.

Underwood, G. M., P. Li, H. Al-Abadleh, and V. H. Grassian (2001), A Knudsen cell study of the heterogeneous reactivity of nitric acid on oxide and mineral dust particles, *J. Phys. Chem. A*, *105*, 6609–6620.

van den Berg, A., F. Dentener, and J. Lelieveld (2000), Modeling the chemistry of the marine boundary layer: Sulfate formation and the role of sea salt aerosol particles, *J. Geophys. Res.*, *105*, 11,671–11,698.

Wang, Y. H., and D. J. Jacob (1998), Anthropogenic forcing on tropospheric ozone and OH since preindustrial times, *J. Geophys. Res.*, *103*, 31,123–31,135.

Wesely, M. L. (1989), Parameterization of surface resistances to gaseous dry deposition in regional-scale numerical models, *Atmos. Environ.*, *23*, 1293–1304.

Wilson, J., C. Cuvelier, and F. Raes (2001), A modeling study of global mixed aerosol fields, *J. Geophys. Res.*, *106*, 34,081–34,108.

Woodward, S. (2001), Modeling the atmospheric life cycle and radiative impact of mineral dust in the Hadley Centre climate model, *J. Geophys. Res.*, *106*, 18,155–18,166.

Zender, C. S., H. Bian, and D. Newman (2003), Mineral Dust Entrainment and Deposition (DEAD) model: Description and 1990s dust climatology, *J. Geophys. Res.*, *108*(D14), 4416, doi:10.1029/2002JD002775.

Zhang, Y., and G. R. Carmichael (1999), The role of mineral aerosol in tropospheric chemistry in East Asia—A model study, *J. Appl. Meteorol.*, *38*, 353–366.

H. Liao and J. H. Seinfeld, Division of Engineering and Applied Science and Department of Chemical Engineering, California Institute of Technology, Pasadena, CA 91125, USA. (seinfeld@caltech.edu)